

Discrete Symmetry Breaking Transitions Between Paired Superfluids

M. J. Bhaseen,¹ S. Ejima,² F. H. L. Essler,³ H. Fehske,² M. Hohenadler,⁴ and B. D. Simons¹

¹*Cavendish Laboratory, University of Cambridge, Cambridge, CB3 0HE, United Kingdom*

²*Institut für Physik, Ernst-Moritz-Arndt-Universität Greifswald, 17489 Greifswald, Germany*

³*The Rudolf Peierls Centre for Theoretical Physics,
University of Oxford, Oxford, OX1 3NP, United Kingdom*

⁴*Institut für Theoretische Physik und Astrophysik,
Universität Würzburg, 97074 Würzburg, Germany*

(Dated: February 28, 2022)

We explore the zero-temperature phase diagram of bosons interacting via Feshbach resonant pairing interactions in one dimension. Using DMRG (Density Matrix Renormalization Group) and field theory techniques we characterize the phases and quantum phase transitions in this low-dimensional setting. We provide a broad range of evidence in support of an Ising quantum phase transition separating distinct paired superfluids, including results for the energy gaps, correlation functions and entanglement entropy. In particular, we show that the Ising correlation length, order parameter and critical properties are directly accessible from a ratio of the atomic and molecular two-point functions. We further demonstrate that both the zero-momentum occupation numbers and the visibility are in accordance with the absence of a purely atomic superfluid phase. We comment on the connection to recent studies of boson pairing in a generalized classical XY model.

PACS numbers: 67.85.Hj, 67.85.Fg, 05.30.Rt

I. INTRODUCTION

The rapid progress in manipulating ultra cold atomic gases has led to new approaches to strongly interacting quantum systems. This includes the properties of highly correlated states of matter, such as Bose–Einstein condensates (BECs) [1, 2], Mott insulators [3], and superfluids [4]. It also allows access to the phase transitions and crossovers between these fascinating phases. In the last few years, the BEC–BCS crossover [5–8] between a molecular BEC and a Bardeen–Cooper–Schrieffer (BCS) pairing state, has stimulated a wealth of experimental activity using fermionic atoms [9–16]. This has been achieved through the use of Feshbach resonances, which enable one to control the strength of pairing interactions using a magnetic field. This has not only opened the door to central problems in condensed matter physics, but also offers insights into the quantum chemistry of molecule formation and chemical reactions [17].

In tandem with these advances, Feshbach resonances and molecule formation have also been studied in bosonic systems [18–26]. Recent experiments have been performed both in optical traps [27–29] and in optical lattices [30]; for a review see Ref. [31]. On the theoretical side, the BEC–BCS “crossover” problem for bosons has also been investigated in the continuum limit [32–34] and on the lattice [35–40]. The problem differs markedly from the fermionic case since the carriers themselves may Bose condense. This leads to the possibility of an Ising quantum phase transition occurring between distinct paired superfluids [32–34]. The phases are distinguished by the presence or absence of carrier condensation, and the associated quantum phase transition involves discrete \mathbb{Z}_2 symmetry breaking. Closely related phases and quantum phase transitions have also been observed in multi-

component fermion systems [41–44], and in the attractive Bose–Hubbard model with a restricted three particle Hilbert space [45–51]. There are also magnetic analogues in quantum spin chains [52]. More recently, the phenomenon of boson pairing has also been explored in the context of a generalized classical XY model with two competing harmonics in the periodic interactions [53–56]. This has led to the prediction of a novel phase diagram with unusual criticality.

Motivated by the possibility of stabilizing pairing phases of bosons [57–62] in cold atomic gases, we recently investigated the bosonic Feshbach resonance problem in one dimension (1D) [63]. We employed large scale DMRG (Density Matrix Renormalization Group) [64] and field theory techniques [63] in order to incorporate the effects of enhanced quantum fluctuations in 1D. Amongst our findings, we presented compelling evidence for an Ising quantum phase transition separating distinct superfluids [65]. The aim of the present manuscript is to shed further light on this novel transition, and to provide a thorough discussion of the superfluid phases in this 1D setting. In particular, we describe a variety of methods to extract the Ising characteristics from the gapless superfluid background. We also provide a quantitative finite-size scaling analysis of the zero-momentum occupation numbers and the visibility. Our results are consistent with the absence of a purely atomic superfluid phase with non-condensed molecules, in contrast to the earlier suggestions of Ref. [37, 38].

The layout of this paper is as follows. In Sec. II we present the Hamiltonian under investigation and in Sec. III we discuss the phase diagram. In Sec. IV we describe the associated field theory and gather our predictions for a variety of local expectation values and correlation functions. We use these results to characterize

the different phases and to establish a detailed comparison with DMRG. In Sec. V we provide a quantitative account of the finite-size scaling of the zero-momentum occupation numbers and the visibility. We contrast our results with those of Refs. [37, 38]. In Sec. VI we discuss the behavior of the entanglement entropy and the emergence of Ising criticality at the transition between the distinct paired superfluids. We also discuss the behavior at the superfluid–Mott insulator transitions. In Sec. VII we describe the Ising scaling regime, and discuss a variety of ways to extract the principal Ising characteristics. This includes the Ising order parameter and the correlation length using a finite-size scaling analysis of the atomic and molecular correlation functions. We also discuss the utility of a suitable ratio of the atomic and molecular two-point functions for analyzing the Ising quantum phase transition. We conclude in Sec. VIII and provide further directions for research.

II. MODEL

We consider the Hamiltonian

$$H = \sum_{i\alpha} \epsilon_{\alpha} n_{i\alpha} - \sum_i \sum_{\alpha} t_{\alpha} \left(b_{i\alpha}^{\dagger} b_{i+1\alpha} + \text{H.c.} \right) + \sum_{i\alpha\alpha'} \frac{U_{\alpha\alpha'}}{2} n_{i\alpha} (n_{i\alpha'} - \delta_{\alpha\alpha'}) + H_{\text{F}}, \quad (1)$$

describing bosons, $b_{i\alpha}$, hopping on a 1D lattice with sites i , where $\alpha = a, m$ labels atoms and molecules [35–40]. Here, ϵ_{α} are on-site potentials, t_{α} are nearest neighbor hopping parameters, and $U_{\alpha\alpha'}$ are interactions. We assume that molecule formation is described by the s-wave Feshbach resonance term,

$$H_{\text{F}} = g \sum_i (m_i^{\dagger} a_i a_i + \text{H.c.}), \quad (2)$$

where we denote $m_i \equiv b_{im}$ and $a_i \equiv b_{ia}$; for recent work on the p-wave problem see Refs. [66, 67]. This conversion implies that the number of atoms and molecules are not separately conserved, but the total, $N_{\text{T}} \equiv \sum_i (n_{ia} + 2n_{im})$, is preserved. For simplicity, in writing Eq. (1) we neglect any effects of higher Bloch bands in optical lattices [68–70]. In this respect, the Hamiltonian (1) may be regarded as a lattice regularization of the continuum models studied in Refs. [32–34]; see also Refs. [24–26]. This approach is very convenient for numerical simulations, and enables us to investigate the superfluid transitions where lattice effects are germane. It also allows us to make contact with previous quantum Monte Carlo (QMC) simulations [37, 38] and to place the problem on a firmer footing. As in the original works [32–34], we neglect the effects of three body losses and finite molecular lifetimes.

In this manuscript we use DMRG on 1D systems with up to $L = 512$ sites, where we set the lattice spacing to

unity and adopt energy units where $t_a = 1$. We furthermore set $t_m = 1/2$ throughout. We work in the canonical ensemble with the total density $\rho_{\text{T}} = N_{\text{T}}/L = 2$ held fixed and allow up to five atoms and five molecules per site, corresponding to a large Hilbert space of dimension $(6 \times 6)^L$; for a discussion of the effects of changing the local Hilbert space dimension see Appendix A. With open (periodic) boundary conditions we retain up to $m_{\rho} = 2400$ ($m_{\rho} = 3000$) states in the density matrix in order to ensure that the discarded weight is less than 1×10^{-10} (1×10^{-8}).

III. PHASE DIAGRAM

As we discussed in Ref. [63], the qualitative phase diagram of the 1D lattice Hamiltonian (1) was previously considered using QMC simulations [37, 38]. In addition to delineating the Mott insulating and superfluid phase boundaries, this work led to intriguing predictions of superfluidity within the Mott phase, and an additional superfluid phase not present in mean field theory [32–36]. Although we find very good quantitative agreement with many of the numerical results [37, 38], these additional predictions are at variance with our recent findings [63] which combine field theory with DMRG. This was also suggested by our earlier studies using hardcore bosons [39, 40]. It has recently been argued that the absence of particle conservation hindered the interpretation of these previous QMC simulations [71]. In this manuscript we will further demonstrate that the use of momentum space observables, including the zero-momentum occupation numbers and the visibility, also complicated the interpretation of these earlier finite-size QMC simulations.

In order to put the problem on a more stable platform, we present a section of the phase diagram in Fig. 1, with parameters chosen for comparison with Ref. [37]. (Note that our conventions differ from Ref. [37] by a factor of 1/2 in the interaction terms so that double occupancy corresponds directly to $U_{\alpha\alpha'}$. Also, ϵ_m plays the role of their detuning parameter, D , when $\epsilon_a = 0$.) The phase boundaries shown in Fig. 1 correspond to the vanishing of the one-particle and two-particle excitation gaps, $E_{1g} \equiv \mu_{1p}(L) - \mu_{1h}(L)$ and $E_{2g} \equiv \mu_{2p}(L) - \mu_{2h}(L)$ respectively, where the data are extrapolated to the thermodynamic limit, $L \rightarrow \infty$. Here

$$\begin{aligned} \mu_{np}(L) &= [E_0(L, N_{\text{T}} + n) - E_0(L, N_{\text{T}})]/n, \\ \mu_{nh}(L) &= [E_0(L, N_{\text{T}}) - E_0(L, N_{\text{T}} - n)]/n, \end{aligned} \quad (3)$$

where $E_0(L, N)$ is the ground state energy for a system of size L and a total number N of atoms and molecules. The phase diagram in Fig. 1 consists of three distinct phases: a Mott insulator (MI) with gaps for both excitations, $E_{1g} \neq 0$ and $E_{2g} \neq 0$, a molecular condensate (MC) with a one-particle gap $E_{1g} \neq 0$ and $E_{2g} = 0$, and a coupled atomic plus molecular condensate (AC+MC) with $E_{1g} = 0$ and $E_{2g} = 0$. As we shall discuss more

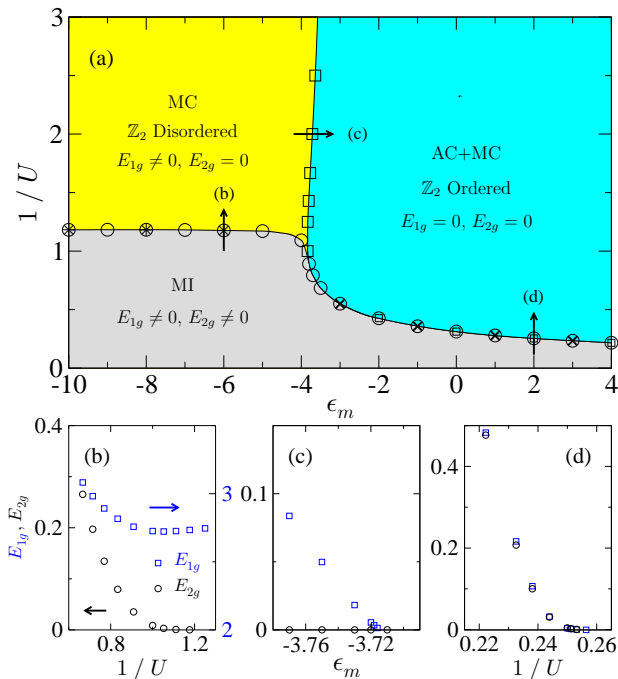


FIG. 1. (color online). (a) Phase diagram of the 1D Hamiltonian (1) with total density $\rho_T = N_T/L = 2$, showing a Mott insulator (MI), a molecular condensate (MC), and a coupled atomic plus molecular condensate (AC+MC). We use DMRG with up to $L = 128$ sites and open boundary conditions. We choose parameters $\epsilon_a = 0$, $U_{aa}/2 = U_{mm}/2 = U_{am} = g = U$, $t_a = 1$, $t_m = 1/2$, for comparison with Ref. [37]. The squares and circles indicate the vanishing of the one-particle and two-particle gaps, E_{1g} and E_{2g} , respectively, as $L \rightarrow \infty$. The stars and crosses indicate where the molecular and atomic correlation exponents, ν_m and ν_a reach $1/4$ in the MC and AC+MC phases respectively. These values correspond to a molecular KT transition and an atomic KT transition respectively. The remaining panels (b), (c) and (d) show the variation of the extrapolated gaps, E_{1g} and E_{2g} with $L \rightarrow \infty$, on passing through the phase boundaries at the corresponding points in panel (a). In particular, we provide detailed evidence for an Ising quantum phase transition occurring between the MC and AC+MC phases.

fully below, the MC phase may be interpreted as a pairing phase of bosons in the absence of atomic condensation. In contrast, the AC+MC phase has both molecular and atomic condensation. In comparison to the qualitative phase diagram presented in Ref. [37], inferred from quantum Monte Carlo simulations on smaller system sizes, we find no evidence for a single-component atomic superfluid phase co-existing with non-condensed molecules. This is in accord with theoretical expectations in higher dimensions, where atomic condensation is always accompanied by molecular condensation [32–34] provided the molecules are present; in the extreme limit where $\epsilon_m \rightarrow \infty$, occurring on the boundary of the AC+MC phase, the molecules are explicitly excluded by the chemical potential as shown in Fig. 2. The conclusions of Ref. [37] have also come under scrutiny due to

the additional claims of superfluidity within the Mott phase [39, 71]. Here, however, our main focus is on the character of the transition between the distinct MC and AC+MC superfluids. In the subsequent discussion we will begin with symmetry arguments and field theory predictions before turning to a comparison with DMRG.

IV. FIELD THEORY DESCRIPTION

A heuristic way to understand the possibility of an Ising quantum phase transition between the distinct MC and AC+MC superfluids is via the generic number-phase relationships, $a \sim \sqrt{\rho_a} e^{i\vartheta_a}$ and $m \sim \sqrt{\rho_m} e^{i\vartheta_m}$, where ρ_a and ρ_m are the average atomic and molecular densities respectively. Substituting these expressions into (1), the Feshbach term (2) takes the form [34]

$$H_F \sim 2g\rho_a\sqrt{\rho_m} \cos(\vartheta_m - 2\vartheta_a). \quad (4)$$

Minimizing this interaction locks the phases of the atomic and molecular condensates according to the relationship

$$\vartheta_m - 2\vartheta_a = \pm\pi, \quad (5)$$

where for simplicity we assume $g > 0$. We see that the phases are locked, but only modulo π , and this gives rise to the possibility of a discrete symmetry breaking Z_2 transition between Feshbach coupled superfluids. Denoting $\vartheta_m \equiv \vartheta$, one may recast the number-phase relationships in the form [34]

$$m \sim \sqrt{\rho_m} e^{i\vartheta}, \quad a \sim \phi e^{i\vartheta/2}, \quad (6)$$

where the Feshbach locking is explicitly enforced and $\phi \sim \sqrt{\rho_a} e^{\mp i\pi/2}$ plays the role of an Ising degree of freedom. The decomposition (6) will play a central role in the subsequent analysis and allows one to gain a handle on the correlation functions and the principal features of the phase diagram.

An alternative way to understand the possibility of an Ising quantum phase transition between the MC and AC+MC phases is via the symmetry of the Hamiltonian (1) under $U(1) \times Z_2$ transformations:

$$m \rightarrow e^{i\theta} m, \quad a \rightarrow e^{i(\theta/2 \pm \pi)} a, \quad (7)$$

where $\theta \in \mathbb{R}$. Before discussing the problem in 1D, where continuous symmetry breaking is absent, we first consider the behavior in higher dimensions [32–34]. In this case, the molecular condensate (MC) phase has $\langle m \rangle \neq 0$ and $\langle a \rangle = 0$. This only breaks the $U(1)$ symmetry, and leaves the Z_2 symmetry, $a \rightarrow -a$, unbroken. This corresponds to an Ising degree of freedom in the disordered phase, coexisting with molecular superfluidity. In contrast, the coupled atomic plus molecular condensate (AC+MC) phase has $\langle m \rangle \neq 0$ and $\langle a \rangle \neq 0$. This breaks the $U(1) \times Z_2$ symmetry completely and corresponds to a Z_2 ordered Ising degree of freedom, coexisting with

atomic and molecular superfluidity. Returning to the present 1D problem, where continuous U(1) symmetry breaking is prohibited, the formation of expectation values for $\langle a \rangle$ and $\langle m \rangle$ is excluded. Instead, superfluidity is characterized by power-law correlations, and the nature of the phases and quantum phase transitions in Fig. 1 requires further examination.

Due to the $U(1) \times \mathbb{Z}_2$ symmetry of the Hamiltonian (1), the low energy Lagrangian of the MC to AC+MC transition is given by $\mathcal{L} = \mathcal{L}_\vartheta + \mathcal{L}_\phi + \mathcal{L}_{\vartheta\phi}$ [34, 72], where

$$\mathcal{L}_\vartheta = \frac{K_\vartheta}{2} [c_\vartheta^{-2}(\partial_\tau\vartheta)^2 + (\partial_x\vartheta)^2] \quad (8)$$

is a free bosonic field and

$$\mathcal{L}_\phi = \frac{K_\phi}{2} [c_\phi^{-2}(\partial_\tau\phi)^2 + (\partial_x\phi)^2] - \mathcal{M}\phi^2 + \lambda\phi^4 \quad (9)$$

is an Ising model in the soft-spin ϕ^4 representation. The coupling between the two sectors, $\mathcal{L}_{\vartheta\phi} = i\phi^2\partial_\tau\vartheta/2$, has a form similar to a Berry phase [34, 72]. A closely related action also arises for tunnelling between quantum wires [73]. In the following we will neglect the contribution $\mathcal{L}_{\vartheta\phi}$ and explore the consequences of the reduced action. Sufficiently far away from the transition this can be justified by a mean-field decoupling, $\mathcal{L}_{\vartheta\phi} \sim i\langle\phi\rangle^2\partial_\tau\vartheta/2$, which reduces the additional interaction to a total derivative term, which can be neglected. The simplified action is therefore expected to provide a good description of the proximate phases. Near the quantum phase transitions, this cannot be neglected *a priori*, and $\mathcal{L}_{\vartheta\phi}$ may change the behavior on very large length scales and in other regions of the phase diagram [73]. However, all of our findings are consistent with expectations based on $\mathcal{L}_\vartheta + \mathcal{L}_\phi$ only. The parameters K_ϑ , c_ϑ , K_ϕ , c_ϕ , η , λ , are related to the coefficients of the Hamiltonian (1), but the details need not concern us here. In this field theory approach, the atoms and molecules are described by the semiclassical number-phase relations given in Eq. (6). In the subsequent discussion we will explore the ramifications of this correspondence in 1D, both for local observables and correlation functions. For complementary work using the Bethe Ansatz and bosonization see also Refs. [74, 75].

A. Local Expectation Values

An immediate consequence of the decomposition (6) is that the densities of atoms and molecules

$$\langle m^\dagger(x)m(x) \rangle \sim \rho_m, \quad \langle a^\dagger(x)a(x) \rangle \sim \langle \phi^2 \rangle, \quad (10)$$

are generically non-zero in both the MC and AC+MC phases. This is supported by our DMRG results as shown in Fig. 2(a). These are extrapolated from the finite-size data to $L \rightarrow \infty$, as indicated in Fig. 2(b). In the limit of large positive detuning with $\epsilon_m \rightarrow \infty$ we have mainly atoms as one would naively expect and $\langle a^\dagger(x)a(x) \rangle \sim 2$. Likewise, in the limit of large negative

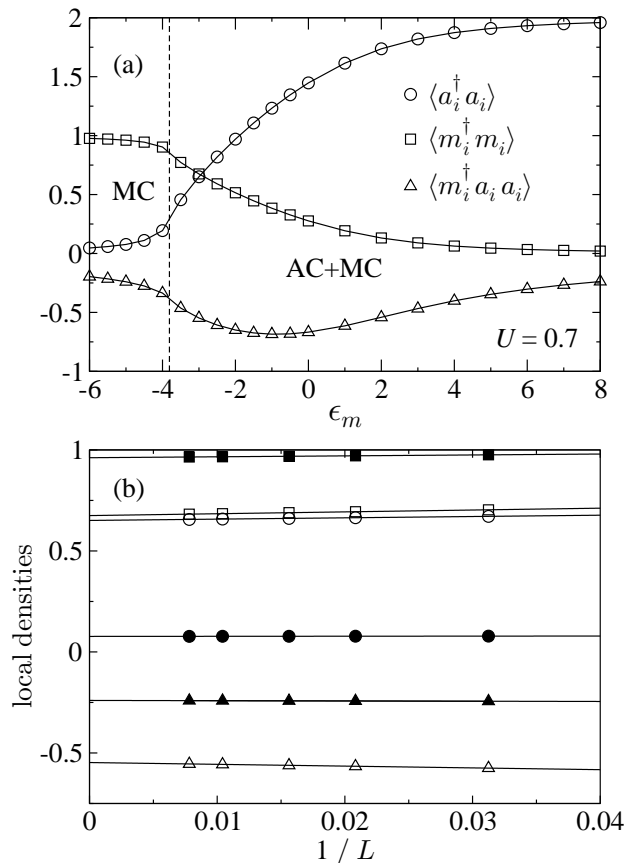


FIG. 2. (a) Local expectation values obtained by DMRG for the 1D Hamiltonian (1) with open boundaries and up to $L = 128$ sites. We use the same parameters as in Fig. 1 and set $U = 0.7$. We plot the local density of atoms $\langle a_i^\dagger a_i \rangle$ (circles), molecules $\langle m_i^\dagger m_i \rangle$ (squares), and the expectation value of the Feshbach conversion term $\langle m_i^\dagger a_i a_i \rangle$ (triangles), evaluated at the system mid-point, $i = L/2$. All of these quantities are generically non-zero on both sides of the MC to AC+MC transition as indicated by the dashed line. In the limit of large positive (negative) detuning ϵ_m we have mainly atoms (molecules) with a density determined by the canonical ensemble constraint $\rho_T = 2$. (b) Corresponding finite-size data and linear extrapolation as a function of $1/L$ for $\epsilon_m = -3$ (open) and $\epsilon_m = -5$ (filled).

detuning, corresponding to $\epsilon_m \rightarrow -\infty$, we have mainly molecules and $\langle m^\dagger(x)m(x) \rangle \sim 1$. These limiting densities are consistent with working in the canonical ensemble with $\rho_T = \sum_i (n_{ia} + 2n_{im})/L = 2$ held fixed.

In addition to these local densities the local expectation value of the Feshbach conversion term,

$$\langle m^\dagger(x)a(x)a(x) \rangle \sim \sqrt{\rho_m} \langle \phi^2 \rangle \neq 0, \quad (11)$$

is non-zero. It exhibits true long range order, even in this low-dimensional setting. This is a consequence of the relevance of the Feshbach term in the renormalization group sense. Our numerical results in Fig. 2 show that this quantity is indeed finite. In particular, this confirms the locking of the phases of the atomic and molecular

condensates (modulo π) on *both* sides of the transition. However, due to the symmetry under $a \rightarrow -a$, the expectation value (11) is naively insensitive to the Ising transition itself, as may be seen in Fig. 2. Further insight into this quantum phase transition and the proximate phases is more readily obtained from correlation functions. We will explore this in more detail below.

B. Green's Functions and Pairing Correlations

The nature of the MC and AC+MC phases shows up most clearly in the atomic and molecular Green's functions, $\langle a^\dagger(x)a(0) \rangle$ and $\langle m^\dagger(x)m(0) \rangle$, and the pairing correlations $\langle a^\dagger(x)a^\dagger(x)a(0)a(0) \rangle$. Their spatial dependence is dictated by the correlations of the underlying Ising model in Eq. (9), and we address each phase in turn.

1. \mathbb{Z}_2 Disordered MC Phase

As follows from the decomposition (6), the molecular Green's function

$$\langle m^\dagger(x)m(0) \rangle \propto \langle e^{-i\vartheta(x)} e^{i\vartheta(0)} \rangle \sim \left(\frac{a_0}{x}\right)^{\nu_m}, \quad (12)$$

decays as a power-law, where the correlation exponent, $\nu_m = 1/(2\pi K_\vartheta)$ varies throughout the phase diagram, and a_0 is a short-distance cutoff. In contrast, in the \mathbb{Z}_2 disordered MC phase, the atomic Green's function

$$\langle a^\dagger(x)a(0) \rangle \propto \langle \phi(x)e^{-i\frac{\vartheta(x)}{2}} \phi(0)e^{i\frac{\vartheta(0)}{2}} \rangle \sim \left(\frac{a_0}{x}\right)^{\frac{\nu_m}{4}} K_0(x/\xi),$$

decays exponentially, where ξ is the Ising correlation length. Here we use the hard-spin fermionic representation of the Ising model to write [76]

$$\langle \phi(x)\phi(0) \rangle \sim K_0(x/\xi), \quad (13)$$

where K_0 is a modified Bessel function. On the other hand, *pairs* of atoms exhibit power-law correlations

$$\langle a^\dagger(x)a^\dagger(x)a(0)a(0) \rangle \sim \left(\frac{a_0}{x}\right)^{\nu_b}, \quad (14)$$

where the exponent $\nu_b = \nu_m$ for these atomic bilinears coincides with the molecular exponent in Eq. (12). That is to say, the MC phase is a pairing phase of bosons without power-law atomic condensation [57–62].

In order to explore these field theory predictions in more detail we perform DMRG on the 1D Hamiltonian (1). The predicted behavior is well supported by our simulations in Fig. 3. The molecules and atomic bilinears show power-law behavior with the same exponent, $\nu_m = \nu_b$, whilst the atomic two-point function shows exponential decay. Our DMRG results also indicate that this behavior persists into the regime close to the Mott insulating phase boundary shown in Fig. 1. In particular, the molecular correlation exponent reaches the value of

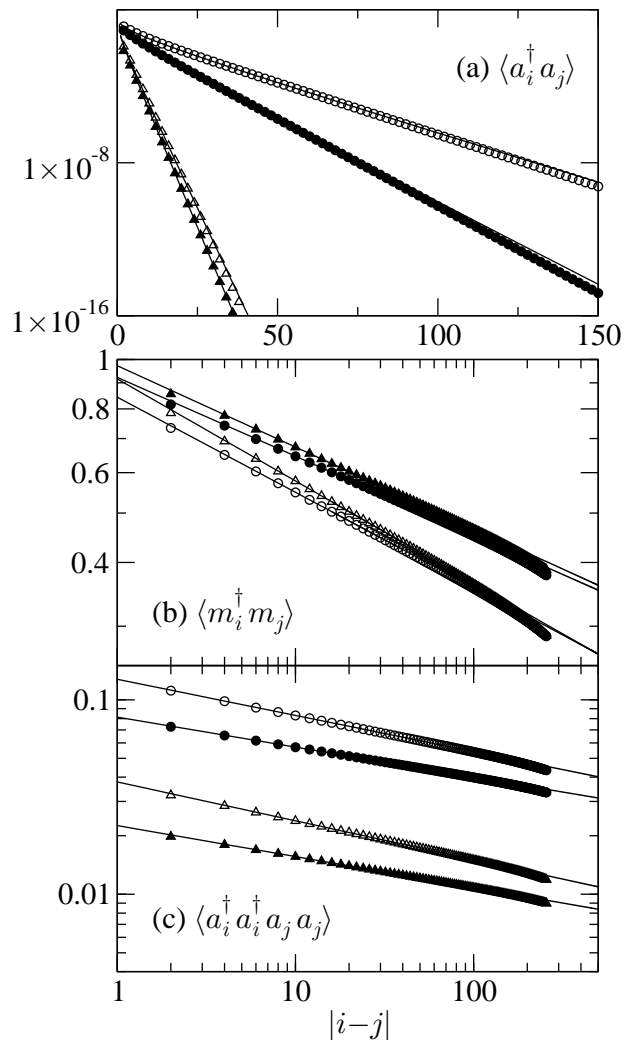


FIG. 3. Correlation functions in the \mathbb{Z}_2 disordered MC phase obtained by DMRG on the 1D Hamiltonian (1) with $L = 512$ and open boundaries. Here and throughout the manuscript we consider sites displaced around the system midpoint in order to minimize boundary effects. We use the same parameters as in Fig. 1 and set $U = 0.7$ (open), $U = 0.5$ (filled), $\epsilon_m = -4$ (circles) and $\epsilon_m = -6$ (triangles). (a) Atomic Green's function $\langle a_i^\dagger a_j \rangle$ showing exponential decay. (b) Molecular Green's function $\langle m_i^\dagger m_j \rangle$ showing power-law behavior. (c) Bilinears of atoms $\langle a_i^\dagger a_i^\dagger a_j a_j \rangle$ showing power-law behavior with the same exponent as the molecular Green's function in panel (b); see Fig. 4. This establishes the MC phase as a pairing phase of atoms without power-law atomic condensation.

$\nu_m = 1/4$ at the MI boundary; see Fig. 4. This is consistent with a molecular Kosterlitz–Thouless (KT) [77, 78] transition. It is analogous to the behavior at the tips of the Mott lobes in the single-band Bose–Hubbard model [79–81] where the Luttinger liquid parameter takes the value $K = 1/(2\pi\nu) = 2/\pi$ in the normalization conventions of Eq. (8). The latter transition takes place at constant density, and is therefore compatible with our

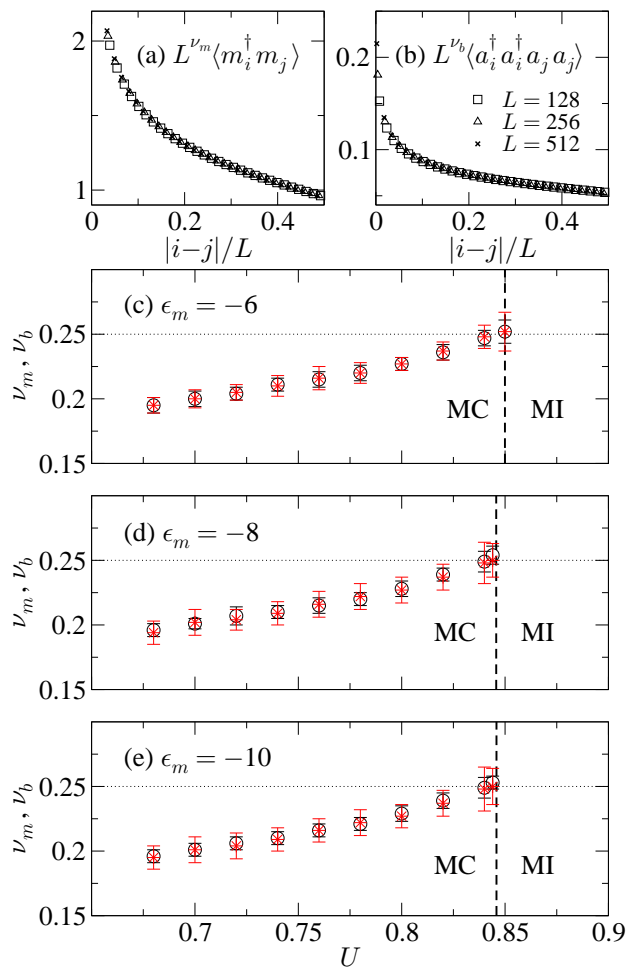


FIG. 4. (color online). DMRG results for the two-point functions of (a) molecules and (b) atomic bilinears in the MC phase with open boundaries and up to $L = 512$. We extract the molecular and bilinear exponents, ν_m and ν_b , by finite-size scaling collapse of the data for different system sizes. In (c), (d) and (e) we show the resulting evolution of ν_m (circles) and ν_b (stars), for vertical scans through Fig. 1 with fixed values of ϵ_m . The vertical dashed lines correspond to the location of the MC to MI transition obtained from the gap data. The molecular exponent reaches the value of $\nu_m = 1/4$ at the MC to MI transition. This corresponds to a molecular KT transition and is analogous to the fixed density transition at the tips of the Mott lobes in the single-band Bose–Hubbard model. The critical exponent ν_b associated with the power-law decay of the atomic bilinears $\langle a_i^\dagger a_i^\dagger a_j a_j \rangle$ (stars) coincides with ν_m .

canonical ensemble constraint, $\rho_T = 2$.

We recall that in deriving the above correlation functions we have neglected the coupling term, $\mathcal{L}_{\partial\phi}$ in the low-energy Lagrangian so that the expressions factorize into independent $U(1)$ and \mathbb{Z}_2 contributions. The good agreement with DMRG lends *a posteriori* support to this approximation within the explored region of the phase diagram.

2. \mathbb{Z}_2 Ordered AC+MC Phase

In the \mathbb{Z}_2 ordered phase the molecular Green’s function

$$\langle m^\dagger(x)m(0) \rangle \propto \langle e^{-i\vartheta(x)} e^{i\vartheta(0)} \rangle \sim \left(\frac{a_0}{x}\right)^{\nu_m}, \quad (15)$$

continues to decay as a power-law. In addition, the atomic Green’s function

$$\langle a^\dagger(x)a(0) \rangle \sim \langle \phi \rangle^2 \langle e^{-i\frac{\vartheta(x)}{2}} e^{i\frac{\vartheta(0)}{2}} \rangle \sim \left(\frac{a_0}{x}\right)^{\nu_a} \quad (16)$$

also decays as a power-law, where the atomic correlation exponent $\nu_a = \nu_m/4$ is locked to the molecular exponent by a factor of one quarter [72]. This is a consequence of the Feshbach coupling which ties the phases of the atomic and molecular condensates together. Note that in writing Eq. (16), we approximate the result for the two-point function of the Ising order parameter at leading order [82]:

$$\langle \phi(x)\phi(0) \rangle \sim \langle \phi \rangle^2 [1 + \pi^{-2}F(x/\xi)] \approx \langle \phi \rangle^2, \quad (17)$$

where

$$F(z) = z^2[K_1^2(z) - K_0^2(z)] - zK_0(z)K_1(z) + \frac{1}{2}K_0^2(z), \quad (18)$$

and $K_0(z)$ and $K_1(z)$ are Bessel functions. These predictions of power-law behavior, as given by Eqs. (15) and (16), are well supported by our numerical simulations as shown in Fig. 5. The locking of the atomic and molecular correlation exponents $\nu_a = \nu_m/4$ is also observed. In addition, these robust features persist into the large- U regime where field theory arguments are no longer strictly valid. In particular, the atomic and molecular correlation functions remain as power-laws right up to the MI boundary shown in Fig. 1. We find that the atomic exponent ν_a reaches the value of $\nu_a = 1/4$ at the AC+MC to MI transition; see Fig. 6. This is consistent with an atomic KT transition, as occurs at the tips of the Mott lobes in the single-band Bose–Hubbard model. At the same time, the molecular exponent ν_m reaches the value of $\nu_m = 1$ due to the aforementioned exponent locking; see Fig. 6. The presence of this molecular superfluid close to the MI boundary, clearly supports the absence of a single component atomic superfluid phase in this 1D setting, in contrast to the findings of Ref. [37]. This is also compatible with mean field theory in higher dimensions [32–34] where atomic condensation is always accompanied by molecular condensation due to the structure of the Feshbach term, H_F . We will return to this issue in Sec. V in our discussion of the corresponding zero-momentum occupation numbers and the visibility.

3. Mixed Correlation Functions

In addition to the purely atomic or molecular Green’s functions, it is also instructive to examine the mixed correlation functions involving both atoms and molecules.

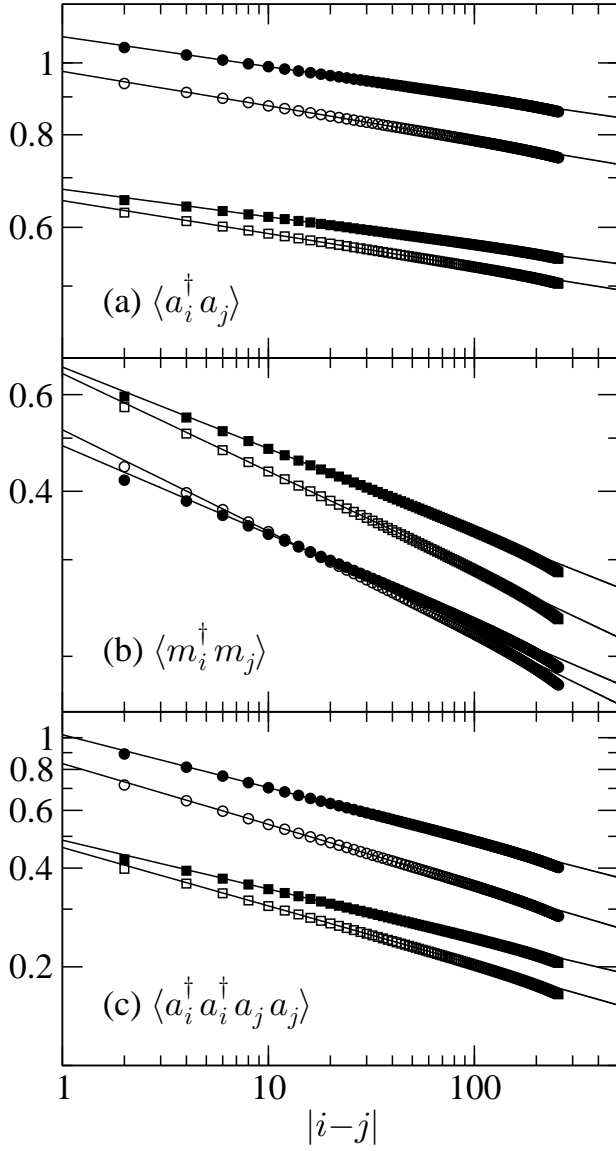


FIG. 5. Correlation functions in the \mathbb{Z}_2 ordered AC+MC phase obtained by DMRG on the 1D Hamiltonian (1) with $L = 512$ and open boundaries. We use the same parameters as in Fig. 1 and set $U = 0.7$ (open), $U = 0.5$ (filled), $\epsilon_m = -2$ (circles) and $\epsilon_m = -3$ (squares). (a) Atomic Green's function $\langle a_i^\dagger a_j \rangle$ showing power-law decay, in contrast to Fig. 3(a). (b) Molecular Green's function $\langle m_i^\dagger m_j \rangle$ showing power-law behavior. The exponent tracks the atomic exponent in (a) up to a factor of 4; see Fig. 6. (c) Bilinears of atoms $\langle a_i^\dagger a_i^\dagger a_j a_j \rangle$ showing power-law behavior with the same exponent as the molecular Green's function in panel (b). This establishes the AC+MC phase as a pairing phase of atoms in the presence of atomic condensation.

It follows from the decomposition (6) that

$$\langle m^\dagger(x)a(0)a(0) \rangle \sim \sqrt{\rho_m} \langle \phi^2 \rangle \left(\frac{a_0}{x} \right)^{\nu_m}, \quad (19)$$

decays as a power-law with the same exponent as the molecular Green's function. Once again, this reflects the

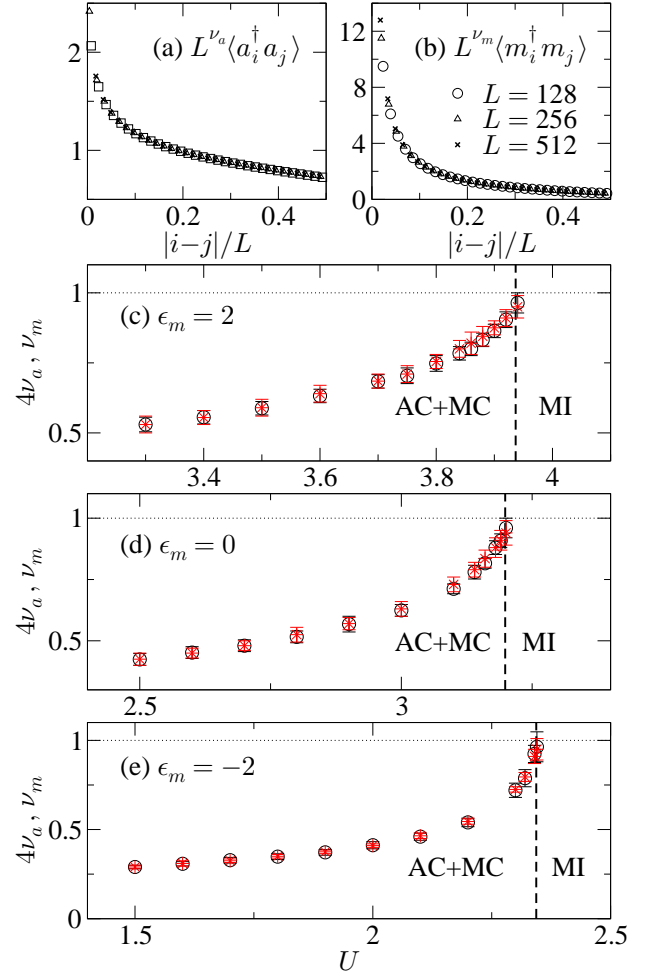


FIG. 6. (color online). DMRG results for the two-point functions of (a) atoms and (b) molecules in the AC+MC phase with open boundaries and up to $L = 512$. We extract the atomic and molecular exponents, ν_a and ν_m , by finite-size scaling collapse of the data for different system sizes. In (c), (d) and (e) we show the resulting evolution of $4\nu_a$ (circles) and ν_m (stars), for vertical scans through Fig. 1 with fixed values of ϵ_m . The vertical dashed lines correspond to the location of the AC+MC to MI transition obtained from the gap data. The data confirm the locking of the atomic and molecular exponents via the relation $\nu_m = 4\nu_a$. The exponents reach the values of $\nu_a = 1/4$ and $\nu_m = 1$ at the MI boundary. This is consistent with an atomic KT transition. It is analogous to the behavior at the tips of the Mott lobes in the single-band Bose-Hubbard model.

phase locking of the atomic and molecular condensates due to the Feshbach term, and is present in both the MC and AC+MC phases. This behavior is in very good agreement with our DMRG simulations as shown in Fig. 7. In particular, the power-law exponent tracks those displayed in Figs. 3(b) and 5(b) for $\langle m^\dagger(x)m(0) \rangle$.

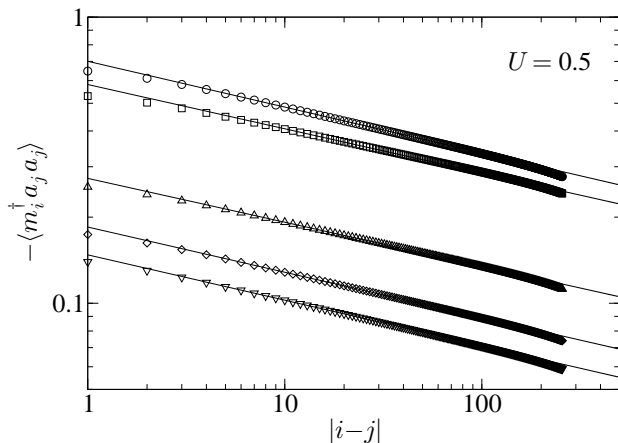


FIG. 7. DMRG results for the mixed correlation function $-\langle m_i^\dagger a_j a_j \rangle$ with $L = 512$ sites, open boundaries and $U = 0.5$. The data correspond to $\epsilon_m = -2$ (circles), $\epsilon_m = -3$ (squares), $\epsilon_m = -4$ (up triangles), $\epsilon_m = -5$ (diamonds), $\epsilon_m = -6$ (down triangles) and show power-law behavior in both the AC and AC+MC phases. As predicted by Eq. (19), the exponents agree with those of the molecular Green's function in panels (b) of Figs. 3 and 5.

C. Density Correlation Functions

Having discussed the atomic and molecular Green's functions we now turn our attention to the correlation functions of the local densities. Denoting $n_m(x) \equiv m^\dagger(x)m(x)$ and $n_a(x) \equiv a^\dagger(x)a(x)$ one obtains

$$\begin{aligned} n_m(x) &\sim \rho_m + \gamma_1 \partial_x \vartheta + \dots, \\ n_a(x) &\sim \rho_a + \gamma_2 \partial_x \vartheta + \gamma_3 : \phi^2(x) : + \dots, \end{aligned} \quad (20)$$

where ρ_m and ρ_a are the average molecular and atomic densities, and $\gamma_1, \gamma_2, \gamma_3$ are constants. Here we use the primary correspondence given in Eq. (6), and combine the exponentials by point-splitting and the short distance operator product expansion. The expansion (20) incorporates the effects of density fluctuations and it follows that the density-density correlations have the same leading dependence in both the MC and AC+MC phases:

$$\langle n_\alpha(x) n_\beta(0) \rangle \simeq \rho_\alpha \rho_\beta + \frac{C_{\alpha\beta}}{x^2} + \dots, \quad (21)$$

where $\alpha, \beta \in a, m$ and $C_{\alpha\beta}$ are non-universal constants. This is confirmed by our DMRG results in Figs. 8 and 9.

V. MOMENTUM SPACE OBSERVABLES

In the previous section we have focused directly on the superfluid correlation functions due to the absence of continuous symmetry breaking in 1D. However, a useful diagnostic of superfluidity in higher dimensions is the

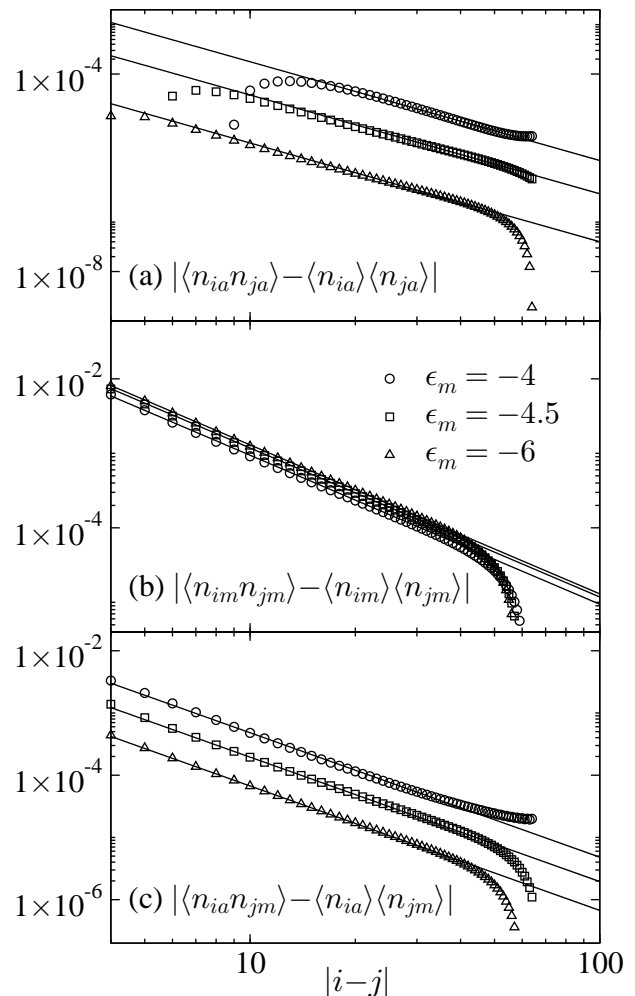


FIG. 8. DMRG results for the connected density correlation functions in the \mathbb{Z}_2 disordered MC phase for the parameters used in Fig. 1. The values of ϵ_m are indicated in panel (b). We use open boundaries with $L = 128$ and set $U = 0.7$. (a) $|\langle n_{ia} n_{ja} \rangle - \langle n_{ia} \rangle \langle n_{ja} \rangle|$. (b) $|\langle n_{im} n_{jm} \rangle - \langle n_{im} \rangle \langle n_{jm} \rangle|$. (c) $|\langle n_{ia} n_{jm} \rangle - \langle n_{ia} \rangle \langle n_{jm} \rangle|$. The results are in agreement with the leading $1/x^2$ dependence predicted by Eq. (21).

divergence of the occupation number

$$n_\alpha(k) = \frac{1}{L} \sum_{i,j=1}^L e^{ik(i-j)} \langle a_{\alpha,i}^\dagger a_{\alpha,j} \rangle \quad (22)$$

at zero momentum, $k = 0$. This quantity was recently used in Ref. [37], in conjunction with visibility data, to argue in favor of a single component atomic superfluid phase in the 1D system (1). In view of our results in the previous sections, which show the presence of both atomic *and* molecular superfluidity right up to the Mott boundary in Fig. 1, we revisit this issue here. As shown in Fig. 6, the atomic and molecular correlation functions in the AC+MC phase are power-laws, $\langle m^\dagger(x)m(0) \rangle \sim x^{-\nu_m}$ and $\langle a^\dagger(x)a(0) \rangle \sim x^{-\nu_m/4}$, with locked exponents. Substituting these asymptotic forms into Eq. (22) suggests

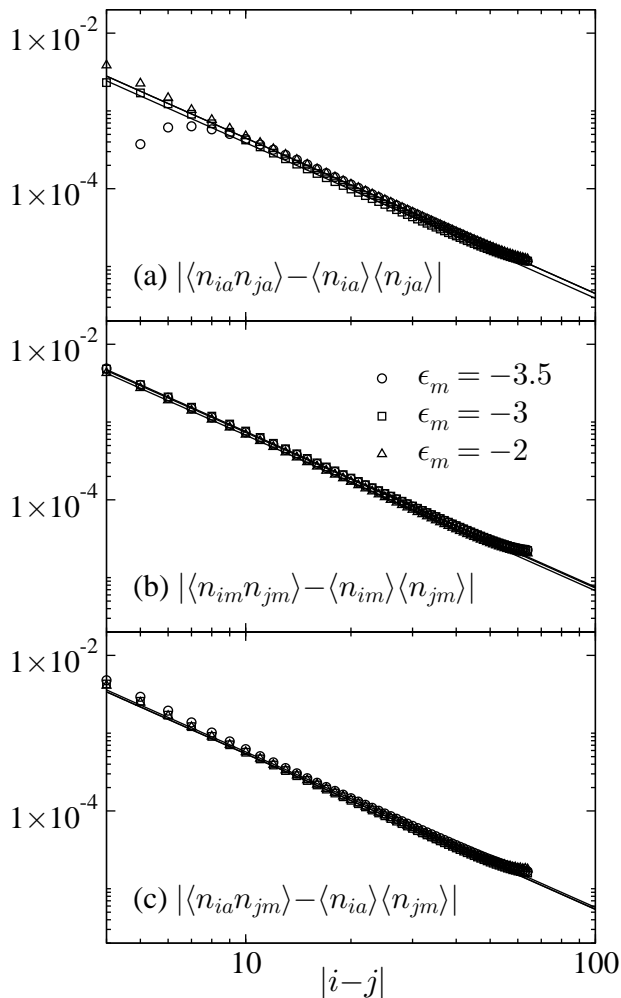


FIG. 9. DMRG results for the connected density correlation functions in the \mathbb{Z}_2 ordered AC+MC phase for the parameters used in Fig. 1. The values of ϵ_m are indicated in panel (b). We use open boundaries with $L = 128$ and set $U = 0.7$. (a) $|\langle n_{ia}n_{ja} \rangle - \langle n_{ia} \rangle \langle n_{ja} \rangle|$. (b) $|\langle n_{im}n_{jm} \rangle - \langle n_{im} \rangle \langle n_{jm} \rangle|$. (c) $|\langle n_{ia}n_{jm} \rangle - \langle n_{ia} \rangle \langle n_{jm} \rangle|$. The results are in agreement with the leading $1/x^2$ dependence predicted by Eq. (21).

that the zero-momentum occupation numbers depend on system size according to [83, 84]

$$n_m(0) \sim \mathcal{A}_m + \mathcal{B}_m L^{1-\nu_m}, \quad n_a(0) \sim \mathcal{A}_a + \mathcal{B}_a L^{1-\nu_m/4}, \quad (23)$$

where $\mathcal{A}_{a,m}$ and $\mathcal{B}_{a,m}$ are constants. In particular, since the molecular exponent, ν_m , only reaches unity at the Mott phase boundary (see Figs. 1 and 6) both of these zero-momentum occupation numbers are expected to diverge with increasing system size. This is supported by our DMRG results as shown in Fig. 10. However, it is evident from Eq. (23) that $n_m(0)$ diverges very slowly with increasing system size close to the MI boundary since $\nu_m \rightarrow 1$. In the absence of a detailed finite-size scaling analysis this may lead to the erroneous conclusion of a purely atomic superfluid. In addition, our findings suggest the absence of any change in behavior in the con-

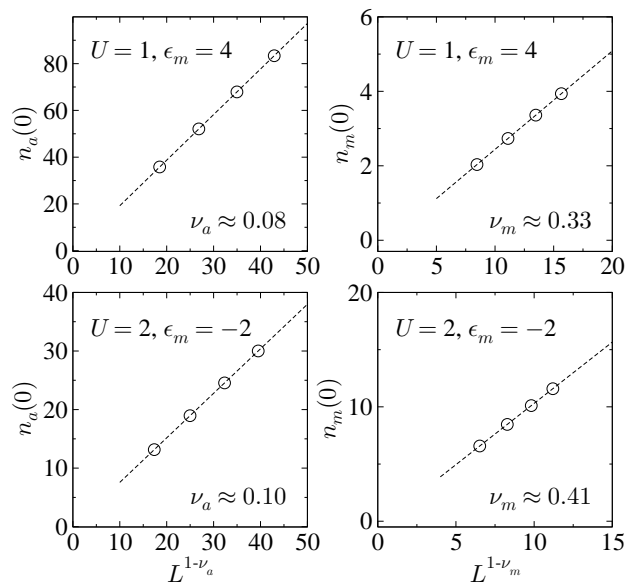


FIG. 10. DMRG results for the dependence of the zero-momentum occupation numbers $n_a(0)$ and $n_m(0)$ on system size L within the AC+MC phase shown in Fig. 1. The results are consistent with algebraic correlations for both atoms and molecules with locked exponents $\nu_m = 4\nu_a$. The presence of molecular superfluidity in the lower panels confirms the absence of an AC phase close to the MI boundary.

vergence properties of $n_m(0)$ as $L \rightarrow \infty$, which could be misinterpreted as a quantum phase transition to a purely atomic superfluid. In general, in this 1D setting, the zero-momentum occupation number is a poor diagnostic of superfluid transitions, since it may simply reflect a change in the *value* of the critical exponent within a superfluid phase, rather than the onset of exponential correlations. Direct evaluation of the correlation functions $\langle a^\dagger(x)a(0) \rangle$ and $\langle m^\dagger(x)m(0) \rangle$ provides a clearer picture in 1D, especially in the case of a finite size system. Our results are fully consistent with the absence of a purely atomic superfluid phase in this region of the phase diagram. This is compatible with the predictions of mean field theory in higher dimensions [32–34].

In addition to the zero-momentum occupation numbers, the authors of Ref. [37] also consider the visibility. The visibility is related to the momentum occupation numbers (22) via [85]

$$\mathcal{V}_\alpha \equiv \frac{n_\alpha^{\max}(k) - n_\alpha^{\min}(k)}{n_\alpha^{\max}(k) + n_\alpha^{\min}(k)}, \quad (24)$$

where n_α^{\max} (n_α^{\min}) is the maximum (minimum) in the momentum space occupation number distribution. In the present context this is identified as

$$\mathcal{V}_\alpha = \frac{n_\alpha(0) - n_\alpha(\pi)}{n_\alpha(0) + n_\alpha(\pi)}. \quad (25)$$

In a superfluid phase where $n_\alpha(0)$ diverges with increasing system size, the visibility \mathcal{V}_α approaches unity as

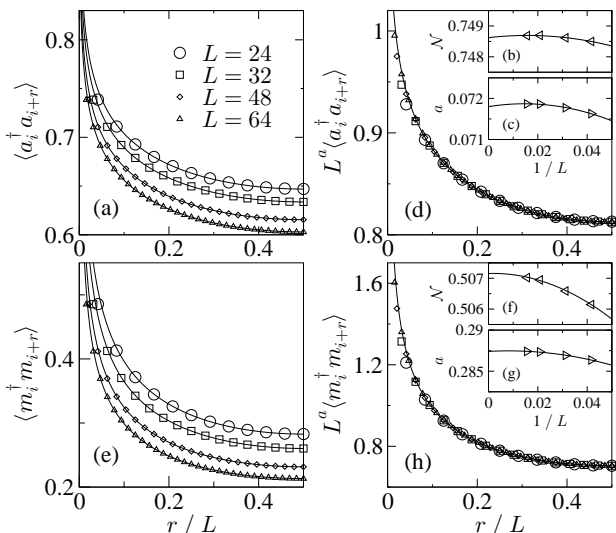


FIG. 11. Atomic and molecular correlation functions within the AC+MC phase obtained by DMRG with periodic boundary conditions. We set $\epsilon_m = -2$ and $U = 1.5$. (a) Atomic correlation function $\langle a_i^\dagger a_{i+r} \rangle$ as a function of the reduced separation r/L for different system sizes. (b) Normalization factor \mathcal{N} obtained from panel (a) using Eq. (26). (c) Correlation exponent a obtained from panel (a) using Eq. (26). (d) Rescaling the data in panel (a) using the extracted exponent a leads to data collapse. This confirms the applicability of the conformal result (26) within the AC+MC phase. This corresponds to power-law atomic correlations for separations $r \gtrsim 3a_0$. The remaining panels show the corresponding results for molecules.

$L \rightarrow \infty$. In Ref. [37] it was argued that the molecular visibility within the AC+MC phase failed to saturate at this value close to the MI boundary. In order to gain a quantitative handle on this issue we need to exploit the finite-size dependence of the superfluid correlations within the AC+MC phase. In a system with periodic boundary conditions the two-point function of a primary field $\mathcal{O}(r)$ at position r can be obtained by conformal transformation [86]:

$$\langle \mathcal{O}(r_1) \mathcal{O}(r_2) \rangle_L = \mathcal{N} \left[\frac{\pi}{L \sin(\frac{\pi r}{L})} \right]^a, \quad (26)$$

where a is the critical exponent in the thermodynamic limit, $r = |r_1 - r_2|$ is the separation, and \mathcal{N} is a constant pre-factor. It follows that the rescaled combination $L^a \langle \mathcal{O}(r_1) \mathcal{O}(r_2) \rangle_L$ is a prescribed scaling function of the reduced separation r/L . The confirmation of this behavior for the atomic and molecular correlation functions within the AC+MC phase is shown in Fig. 11. Given this agreement we may substitute the conformal result (26) into Eq. (22) in order to obtain formal expressions for the finite-size dependence of the atomic and molecular visibilities in Eq. (24). In Fig. 12 we show the results of this conformal extrapolation, where we further incorporate the exact DMRG results for the short distance behavior with $r \leq 3a_0$, where a_0 is the lattice spacing. It

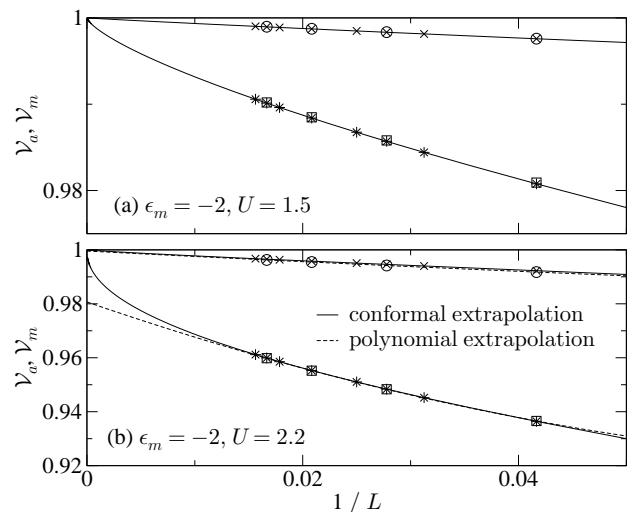


FIG. 12. Finite-size scaling of the atomic and molecular visibilities within the AC+MC phase. The circles correspond to \mathcal{V}_a and the squares to \mathcal{V}_m obtained by Fourier transformation of the correlation functions obtained by DMRG. The crosses and stars correspond to Fourier transformation of the conformal result (26) supplemented by exact DMRG results for the correlators at small separations $r \leq 3a_0$. The solid line indicates the results of conformal extrapolation (described in the text and justified by the scaling collapse in Fig. 11) supplemented by the exact DMRG results for small separations $r \leq 3a_0$. (a) With $\epsilon_m = -2$ and $U = 1.5$ both \mathcal{V}_a and \mathcal{V}_m extrapolate to unity in the thermodynamic limit. (b) Close to the MI transition with $\epsilon_m = -2$ and $U = 2.2$ both \mathcal{V}_a and \mathcal{V}_m approach unity as $L \rightarrow \infty$. This is in direct contrast to naive polynomial extrapolation (dashed) which erroneously suggests that the molecular visibility is less than unity.

is readily seen from the solid lines in Fig. 12 that both the atomic and molecular visibilities extrapolate to unity in the thermodynamic limit. In particular, close to the MI boundary there are strong deviations from the results that would be obtained by naive polynomial extrapolation as indicated by the dashed lines. In Fig. 13(a) we use the conformal extrapolation procedure to track the atomic and molecular visibilities within the AC+MC phase. The results are consistent with unity right up to the MI boundary. For comparison, in Fig. 13(b) we show the results that would be inferred using a naive polynomial extrapolation. The results are in accordance with those of Ref. [37], but differ markedly from the asymptotic visibilities obtained by conformal extrapolation as shown in Fig. 13(a).

To summarize the results of this section, within the AC+MC phase the finite-size dependence of the atomic and molecular momentum space diagnostics is in complete agreement with power-law correlations for both the atoms and the molecules. This behavior persists right up to the MI boundary and provides further evidence for the absence of a purely AC phase. This is analogous to expectations in higher dimensions arising from mean-field theory analyses [32–34].

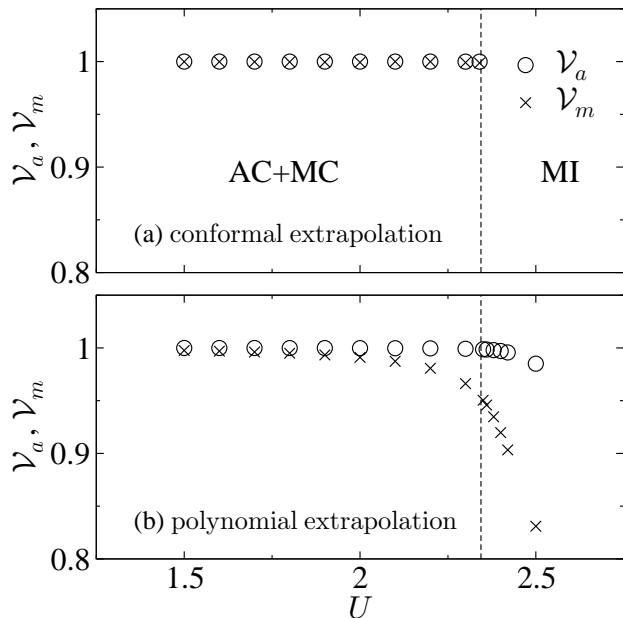


FIG. 13. (a) Atomic and molecular visibilities \mathcal{V}_a (circles) and \mathcal{V}_m (crosses) within the AC+MC phase for $\epsilon_m = -2$ obtained by DMRG with up to $L = 64$ and periodic boundaries. We use the conformal extrapolation procedure described in the text in order to obtain the asymptotic results as $L \rightarrow \infty$. Both \mathcal{V}_a and \mathcal{V}_m are unity right up to the MI boundary, indicating the presence of both atomic and molecular superfluidity. (b) Naive polynomial extrapolation erroneously suggests that the molecular visibility is less than unity in the AC+MC phase.

VI. ENTANGLEMENT ENTROPY

Having established good agreement between field theory and DMRG for the MC and AC+MC phases, let us now examine the quantum phase transition between them. A key diagnostic in this 1D setting is the central charge, c , which is a measure of the number of critical degrees of freedom. This may be obtained from the entanglement entropy. For a block of length l in a periodic system of length L , the von Neumann entropy is given by $S_L(l) = -\text{Tr}_l(\rho_l \ln \rho_l)$, where $\rho_l = \text{Tr}_{L-l}(\rho)$ is the reduced density matrix. One obtains [87, 88]

$$S_L(l) = \frac{c}{3} \ln \left[\frac{L}{\pi} \sin \left(\frac{\pi l}{L} \right) \right] + s_1 + \dots, \quad (27)$$

where s_1 is a non-universal constant and where the corrections are small when the chord length is large [89–95]. As may be seen in Fig. 14(a), the numerically extracted central charge of the MC phase yields $c = 1$, as one would expect for a single free boson, with coexisting gapped degrees of freedom; the adjacent panel shows the same results plotted against the conformal distance $\tilde{l} \equiv \ln[(L/\pi) \sin(\pi l/L)]$ in order to yield a linear slope of $c/3$. It may be seen from Fig. 14(c) that the AC+MC phase also has $c = 1$. Note that it is *not* $c = 2$ as would be the case for two independent Luttinger liquids. This

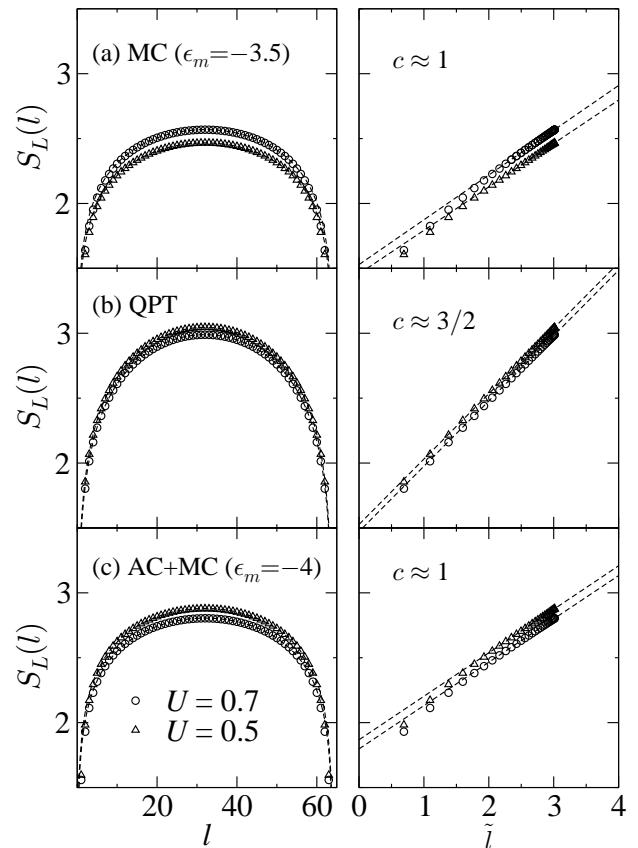


FIG. 14. Entanglement entropy $S_L(l)$ obtained by DMRG with $L = 64$ and periodic boundaries. We consider horizontal scans through Fig. 1 with $U = 0.5$ and $U = 0.7$. (a) Within the MC phase with $\epsilon_m = -3.5$ we find $c \approx 1$ corresponding to a gapless superfluid. (b) In the vicinity of the MC to AC+MC quantum phase transition we find $c \approx 3/2$. This corresponds to the presence of additional gapless Ising degrees of freedom coexisting with superfluidity. (c) Within the AC+MC phase with $\epsilon_m = -4$ we find $c \approx 1$ corresponding to an effective free boson. The panels on the left, but are plotted against the conformal distance $\tilde{l} \equiv \ln[(L/\pi) \sin(\pi l/L)]$ in order to yield a linear plot with slope $c/3$. The offset between the different curves within each panel is due to the non-universal contribution in Eq. (27).

reflects the coupled nature of the atomic and molecular condensates in the AC+MC phase, with additional gapped Ising degrees of freedom; the Feshbach term is relevant and drives the \mathbb{Z}_2 sector massive. Close to the MC to AC+MC transition, where the anticipated Ising gap closes, one expects the central charge to increase to $c = 3/2$, due to *additional* critical Ising degrees of freedom with $c = 1/2$. This is confirmed by our DMRG simulations in Fig. 14(b). Further support for this \mathbb{Z}_2 transition is obtained from the difference [96],

$$\Delta S(L) \equiv S_L(L/2) - S_{L/2}(L/4) = \frac{c}{3} \ln(2) + \dots, \quad (28)$$

as a function of ϵ_m . For a given system size this displays a peak, whose location coincides with the MC to AC+MC

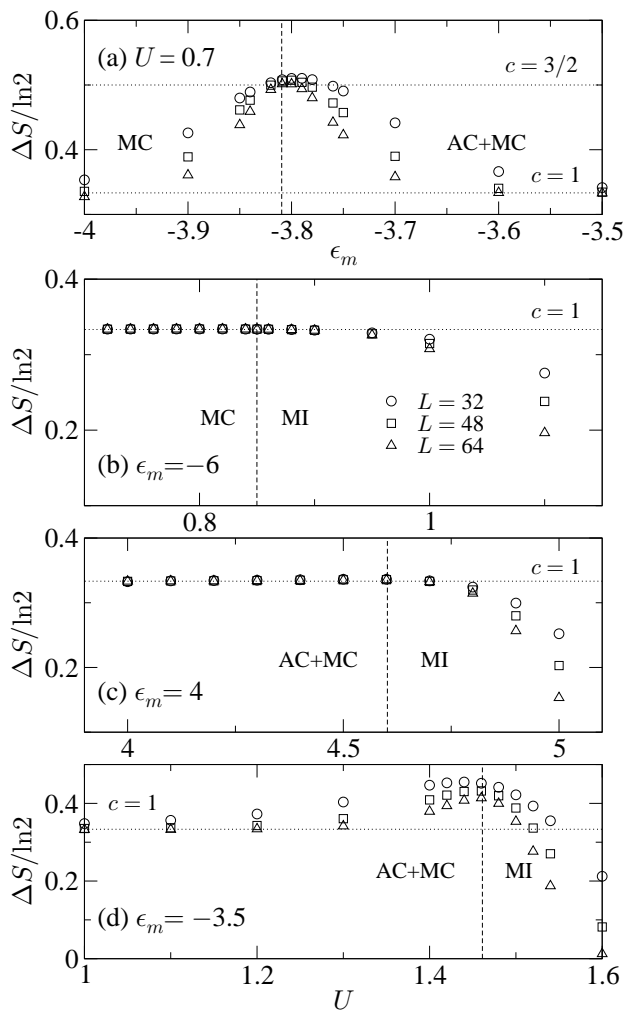


FIG. 15. Entanglement entropy difference $\Delta S(L)$ on transitioning across the phase boundaries shown in Fig. 1. We use periodic boundaries with up to $L = 64$ and work away from the multicritical point. (a) The transition from MC to AC+MC yields $c \approx 3/2$ corresponding to an Ising transition coexisting with a gapless superfluid. (b) The transition from MC to MI yields $c \approx 1$ and is consistent with a molecular KT transition. (c) The transition from AC+MC to MI with $\epsilon_m = 4$ yields $c \approx 1$ and is consistent with an atomic KT transition. (d) The transition from AC+MC to MI with $\epsilon_m = -3.5$ appears to be compatible with the approach towards $c \approx 1$ with increasing L , although the finite-size effects are stronger than those in panel (c). Panels (a) and (c) are adapted from Ref. [63].

quantum phase transition obtained via the vanishing of the single-particle gap, $E_{1g} = 0$, as shown in Fig. 1; see Fig. 15(a). The evolution with increasing system size is consistent with the passage towards $c = 1$ in the superfluid phases, and $c = 3/2$ in the vicinity of the transition. This behavior may be contrasted with that observed at the superfluid-MI transitions in Fig. 1, away from the multicritical point. As may be seen in Fig. 15(b), in passing from the MC phase to the MI, the central charge remains pinned at unity. This is consistent with a KT

transition for the molecules. Likewise, in passing from the AC+MC phase to the MI, we find $c = 1$ again; see Fig. 15(c). This is consistent with a KT transition for the atoms. We have checked that this atomic KT behavior persists in Fig. 1 up to a value of $\epsilon_m = -3.5$; see Fig. 15(d). It is notable that the finite-size effects in Fig. 15(d) are much stronger than those in Fig. 15(c), although both are compatible with $c \approx 1$ at the MI transition. A detailed analysis of the multicritical region in Fig. 1 requires further investigation.

VII. ISING SCALING REGIME

Having provided evidence for a \mathbb{Z}_2 quantum phase transition occurring between the MC and AC+MC superfluids, we now demonstrate how to extract both the Ising order parameter, $\langle \phi \rangle$, and the Ising correlation length, ξ , in the presence of the additional superfluid degrees of freedom with $c = 1$.

A. Ising Correlation Length

The Ising correlation length, ξ , may be obtained from the atomic and molecular correlation functions discussed in Sec. IV B. Within the \mathbb{Z}_2 disordered MC phase the atomic correlations $\langle a^\dagger(x)a(0) \rangle \sim x^{-\nu_m/4} K_0(x/\xi)$ decay exponentially, whilst the molecular correlations $\langle m^\dagger(x)m(0) \rangle \sim x^{-\nu_m}$ decay as a power-law. At a given point in parameter space we may use the molecular Green's function to determine the exponent ν_m , and thereby extract the Ising correlation length from the atomic correlations. This approach is outlined in Fig. 16. In the vicinity of an Ising quantum phase transition one expects that $\xi^{-1} \sim |\mathcal{M} - \mathcal{M}_c|^\nu$ where $\nu = 1$ is the Ising correlation length exponent and \mathcal{M} is a suitable mass scale parameterizing the departure from criticality. Unfortunately, it is non-trivial to express \mathcal{M} in terms of the microscopic parameters of the lattice model (1). A naive analysis gives $\mathcal{M} \sim \kappa_0 + \kappa_1 \rho_m + \kappa_2 \sqrt{\rho_m}$, where ρ_m is the density of molecules, and $\kappa_0 \sim \epsilon_a$, $\kappa_1 \sim U_{am}$, $\kappa_2 \sim 2g$ are constants. Expanding the square root according to $\sqrt{\rho_m} \approx \sqrt{\rho_m^c} + (\rho_m - \rho_m^c)/\sqrt{\rho_m^c}$ suggests that sufficiently close to the Ising transition

$$\xi^{-1} \propto |\rho_m - \rho_m^c|. \quad (29)$$

This Ising behavior with $\nu = 1$ is confirmed in Fig. 16.

B. Ising Order Parameter

In the ordered phase of the Ising model (9) we have $\langle \phi \rangle \sim |\mathcal{M} - \mathcal{M}_c|^\beta$ where $\beta = 1/8$ is the Ising magnetization critical exponent. From the discussion above one thus expects that

$$\langle \phi \rangle \sim |\rho_m - \rho_m^c|^{1/8}, \quad (30)$$

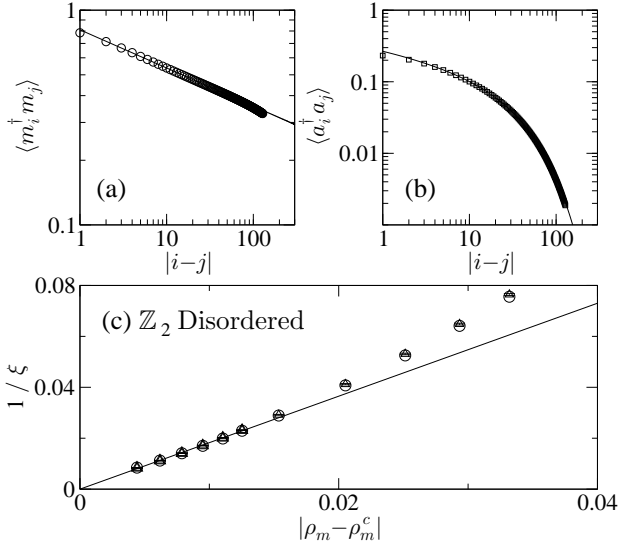


FIG. 16. DMRG results used to extract the Ising correlation length ξ within the \mathbb{Z}_2 disordered MC phase with $L = 256$ and open boundaries. (a) With $\epsilon_m = -3.85$ the molecular correlation function $\langle m_i^\dagger m_j \rangle \approx 0.81|i-j|^{-0.18}$ decays as a power-law. (b) Using the previous exponent $\nu_m \approx 0.18$ we extract the Ising correlation length $\xi \approx 43.6$ from the exponential decay of $\langle a_i^\dagger a_j \rangle \sim |i-j|^{-\nu_m/4} K_0(|i-j|/\xi)$. (c) Repeating the above procedure we plot ξ^{-1} (circles) versus the departure of the molecular density ρ_m from its value ρ_m^c at the MC to AC+MC transition. Close to the transition the results are in good agreement with the Ising relation $\xi^{-1} \sim |\rho_m - \rho_m^c|^\nu$ with $\nu = 1$. The triangles correspond to extracting ξ directly from the ratio $\mathcal{R}(|i-j|) \equiv \langle a_i^\dagger a_j \rangle^4 / \langle m_i^\dagger m_j \rangle \sim [K_0(|i-j|/\xi)]^4$.

where ρ_m is the density of molecules. In order to test the validity of Eq. (30), we must first extract the Ising order parameter from a finite-size scaling analysis of the atomic correlations. As follows from Eq. (16), within the \mathbb{Z}_2 ordered AC+MC phase one has

$$\langle a^\dagger(x)a(0) \rangle = \mathcal{A}\langle\phi\rangle^2 x^{-\nu_m/4}, \quad (31)$$

where \mathcal{A} is a normalization amplitude. In Fig. 17(a) we show DMRG results for $\langle a^\dagger(x)a(0) \rangle$ in the vicinity of the MC to AC+MC quantum phase transition. A direct fit to Eq. (31) yields $\mathcal{A}\langle\phi\rangle^2$. Repeating this procedure for different system sizes one obtains an estimate for $\mathcal{A}\langle\phi\rangle^2$ in the thermodynamic limit; see Fig. 17(b). In Fig. 18 we show the variation of this order parameter with the molecular density. The results are in good agreement with the theoretical prediction in Eq. (30) and the Ising critical exponent $\beta = 1/8$.

C. Correlation Function Ratio

In the above discussion we have extracted the Ising correlation length and the Ising order parameter through a direct finite-size scaling analysis of the atomic and molecular correlation functions. An alternative approach is to

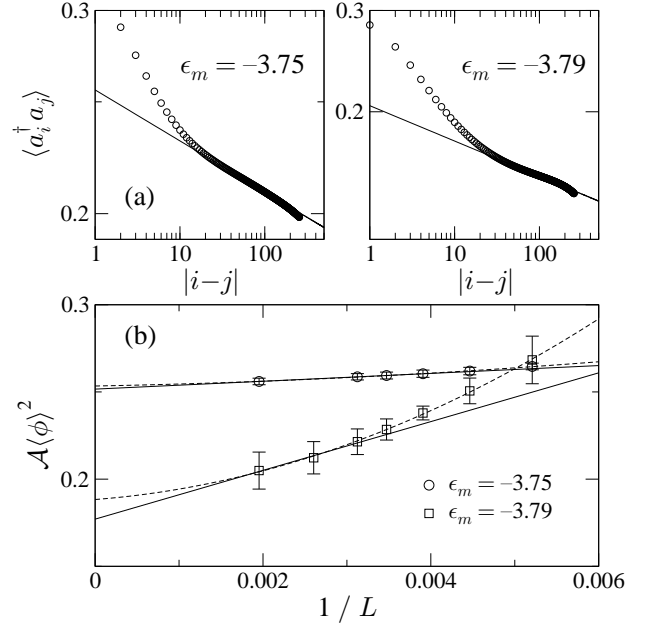


FIG. 17. (a) Atomic correlation functions within the AC+MC phase obtained by DMRG with up to $L = 512$ and open boundaries. We set $U = 0.7$ and consider $\epsilon_m = -3.75$ (left) and $\epsilon_m = -3.79$ (right). A direct fit to Eq. (31) yields $\mathcal{A}\langle\phi\rangle^2$ for each value of ϵ_m , where $\langle\phi\rangle$ is the Ising order parameter and \mathcal{A} is a non-universal constant prefactor. Changing the fitting interval gives an estimate of the error bars. (b) Extrapolation of $\mathcal{A}\langle\phi\rangle^2$ to the thermodynamic limit using linear extrapolation of the largest three system sizes is indicated by the solid line. An estimate of the error bars in the thermodynamic limit is obtained by comparing to a quadratic fit of the data shown by the dashed line. These results are plotted as a function of the molecular density in Fig. 18 in order to confirm Ising behavior with $\beta = 1/8$.

consider the behavior of the ratio

$$\mathcal{R}(x) \equiv \frac{\langle a^\dagger(x)a(0) \rangle^4}{\langle m^\dagger(x)m(0) \rangle}, \quad (32)$$

in analogy to the considerations of Refs. [42, 43] for the confinement-deconfinement transition of Cooper pairs in 1D fermion systems.

In the \mathbb{Z}_2 disordered MC phase $\langle a^\dagger(x)a(0) \rangle \sim x^{-\nu_m/4} K_0(x/\xi)$ and $\langle m^\dagger(x)m(0) \rangle \sim x^{-\nu_m}$. It follows that the power-law prefactors cancel out in this ratio:

$$\mathcal{R}(x) \sim [K_0(x/\xi)]^4. \quad (33)$$

As such, this ratio should exhibit exponential decay in the MC phase. This is confirmed by our DMRG results in Fig. 19(a). A direct fit to Eq. (33) yields the Ising correlation length shown by the triangles in Fig. 16.

In the \mathbb{Z}_2 ordered AC+MC phase $\langle m^\dagger(x)m(0) \rangle \sim x^{-\nu_m}$ and $\langle a^\dagger(x)a(0) \rangle \sim \langle \phi(x)\phi(0) \rangle x^{-\nu_m/4}$ where $\langle \phi(x)\phi(0) \rangle$ is given by Eq. (17). It follows that

$$\mathcal{R}(x) \sim \langle \phi \rangle^8 [1 + \pi^{-2} F(x/\xi)]^4, \quad (34)$$

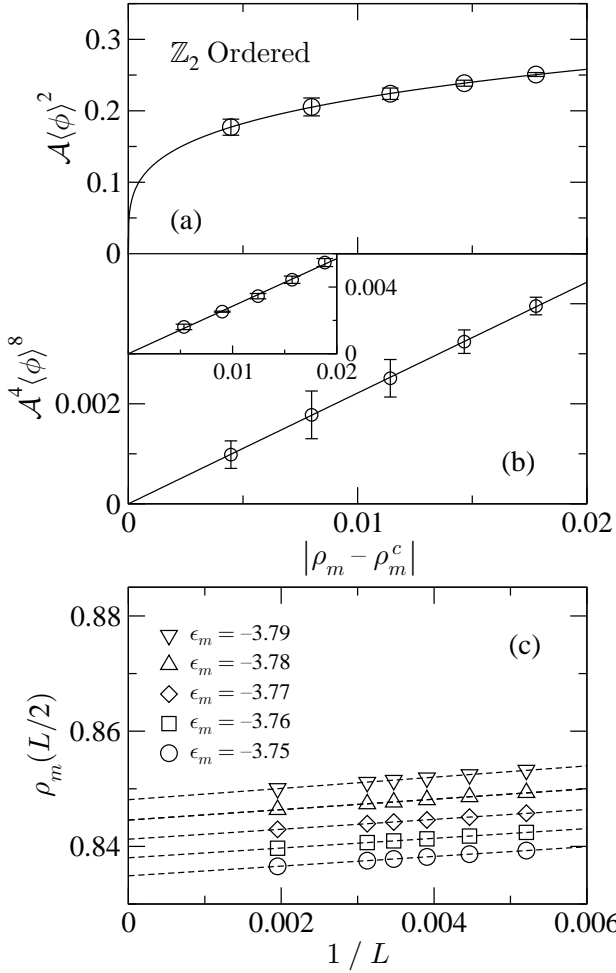


FIG. 18. DMRG results for the Ising order parameter in the \mathbb{Z}_2 ordered AC+MC phase with up to $L = 512$ and $U = 0.7$. (a) Variation of the Ising order parameter squared $\mathcal{A}\langle\phi\rangle^2$ where \mathcal{A} is a constant prefactor, versus the deviation of the molecular density ρ_m from its value ρ_m^c at the MC to AC+MC quantum phase transition. (b) Variation of $\mathcal{A}^4\langle\phi\rangle^8$ versus the molecular density difference. The results are in good agreement with the Ising magnetization relation $\langle\phi\rangle \sim |\rho_m - \rho_m^c|^{1/8}$ with $\beta = 1/8$. The inset shows analogous results obtained from the plateau value of $\mathcal{R}(x)$ for $L = 512$, as indicated in Fig. 19(c). The error bars are estimated from the magnitude of $|\mathcal{R}(x = 128, L = 512) - \mathcal{R}(x = 64, L = 256)|$. (c) Finite-size scaling of the thermodynamic molecular density used in panels (a) and (b). Panels (a) and (b) are adapted from Ref. [63].

where $F(z)$ is given by Eq. (18). At leading order $\mathcal{R}(x) \sim \langle\phi\rangle^8$ and one thus expects $\mathcal{R}(x)$ to develop a constant plateau that is proportional to the Ising order parameter. This is confirmed by our DMRG results in Fig. 19(c).

In addition to these results for $\mathcal{R}(x)$ which are valid within the superfluid phases, one may also explore the vicinity of the quantum phase transition between them. At the Ising critical point $\langle\phi\rangle = 0$ but

$$\langle\phi(x)\phi(0)\rangle \sim \left(\frac{a_0}{x}\right)^\eta, \quad (35)$$

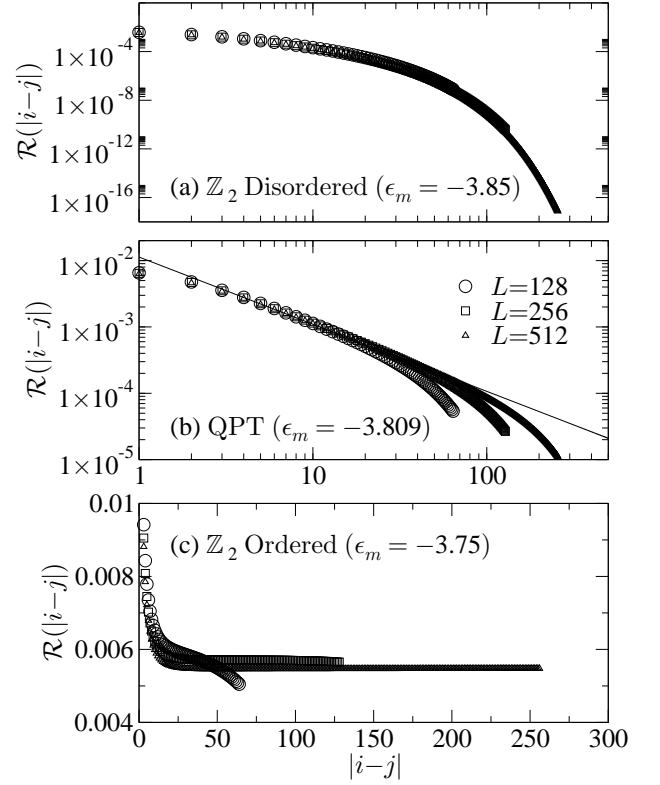


FIG. 19. Ratio $\mathcal{R}(|i-j|) \equiv \langle a_i^\dagger a_j \rangle^4 / \langle m_i^\dagger m_j \rangle$ of the atomic and molecular correlation functions with $U = 0.7$. (a) In the \mathbb{Z}_2 disordered MC phase with $\epsilon_m = -3.85$ the ratio $\mathcal{R}(|i-j|) \sim [K_0(|i-j|/\xi)]^4$ exhibits exponential decay. (b) In the vicinity of the MC to AC+MC quantum phase transition the ratio $\mathcal{R}(|i-j|) \sim 1/|i-j|$ decays with a universal power-law corresponding to the Ising critical exponent $\eta = 1/4$. The line is a fit to $\mathcal{R} = A_0|i-j|^{-A_1}$ over the interval $3 \leq |i-j| \leq 48$ for $L = 512$ with $A_0 \approx 0.011$ and $A_1 \approx -1.01$. (c) In the \mathbb{Z}_2 ordered AC+MC phase with $\epsilon_m = -3.75$ the ratio $\mathcal{R}(|i-j|) \sim \langle\phi\rangle^8$ exhibits a plateau corresponding to a non-zero Ising order parameter.

decays as a power-law where $\eta = 1/4$ is the Ising pair correlation exponent. It follows from Eqs. (6) and (35) that the atomic Green's function at criticality is given by

$$\begin{aligned} \langle a^\dagger(x)a(0) \rangle &\sim \langle \phi(x)\phi(0) \rangle \langle e^{-i\frac{\vartheta(x)}{2}} e^{i\frac{\vartheta(0)}{2}} \rangle \\ &\sim \left(\frac{a_0}{x}\right)^{\frac{1}{4}} \left(\frac{a_0}{x}\right)^{\frac{\nu_m}{4}}. \end{aligned} \quad (36)$$

On passing from the \mathbb{Z}_2 ordered AC+MC phase towards the Ising quantum phase transition, the power-law decay of the atomic Green's function is therefore enhanced by $\eta = 1/4$ due to the presence of additional critical Ising degrees of freedom. It follows that

$$\mathcal{R}(x) \sim \frac{a_0}{x}, \quad (37)$$

exhibits universal power-law decay in the vicinity of the MC to AC+MC quantum phase transition. This is confirmed by our DMRG results shown in Fig. 19(b). This

provides direct evidence for the Ising correlation exponent, $\eta = 1/4$. These results demonstrate that the ratio $\mathcal{R}(x)$ may be used to explore both the critical and off-critical Ising behavior at the MC to AC+MC transition. The characteristic signatures of $\mathcal{R}(x)$ parallel those observed in Refs. [42, 43] for the confinement-deconfinement transition of Cooper pairs in 1D fermion systems.

VIII. CONCLUSIONS

In this manuscript we have explored the phase diagram of bosons interacting via Feshbach resonant pairing in a 1D optical lattice. We have presented a wide variety of evidence in favor of an Ising quantum phase transition separating distinct paired superfluids. We have also provided a detailed characterization of these phases, including the behavior close to the Mott insulating phase boundary. For the investigated parameters, our DMRG results are consistent with an Ising quantum phase transition approaching both a molecular KT transition and an atomic KT transition. This is compatible with mean field theory predictions for the continuum model in higher dimensions. However, recent results for pairing phases in a 2D classical XY model suggest the possibility that the Ising transition may over-extend beyond the multicritical point [53]. In view of this possibility, in a distinct but closely related model, it would be profitable to explore the multicritical region in more detail. A clear verdict on this issue for the present 1D quantum model requires further analytical and numerical investigation and we will return to this question in future work. It would also be interesting to explore the phase diagram for a broader range of parameters, with a specific focus on the choice of atomic species and experimental constraints. Even in the presence of strong three body losses, the emergent phase diagram may exhibit notable similarities [45–51].

ACKNOWLEDGMENTS

We are grateful to E. Altman, F. Assaad, S. Capponi, N. Cooper, S. Diehl, M. Garst, Z. Hadzibabic, A. James, E. Jeckelmann, J. Kjäll, M. Köhl, A. Lamacraft, A. Läuchli, C. Lobo, J. Moore, N. Prokof'ev, A. Silver and M. Zaletel for helpful comments and discussions. MJB and BDS acknowledge EPSRC grant no. EP/E018130/1. FHLE by EP/I032487/1 and EP/D050952/1. SE and HF acknowledge funding by the DFG through grant SFB 652. MH by DFG FG1162. Numerical calculations were performed at the URZ Greifswald.

Appendix A: Hilbert Space Truncation

Throughout the main text we truncate the local Hilbert space to allow up to a maximum of $n_a = 5$ atoms and $n_m = 5$ molecules per site. In the regime of large

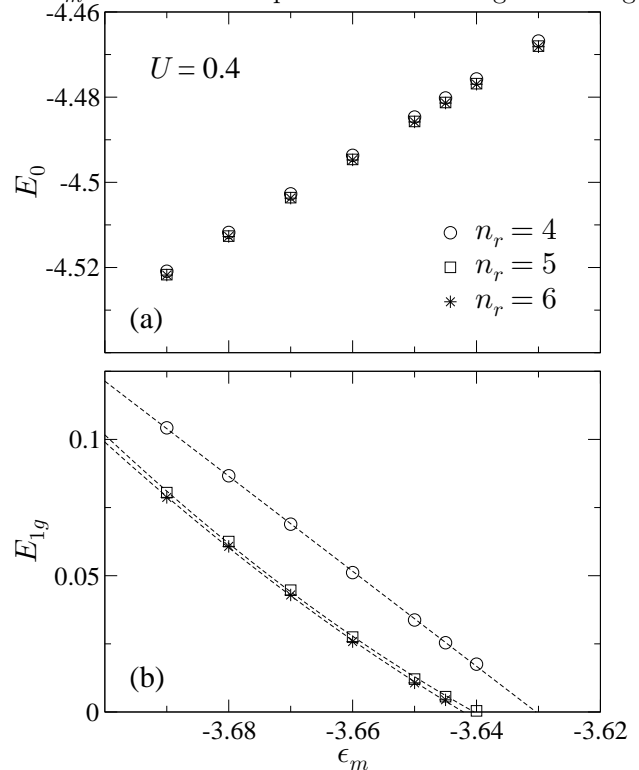


FIG. 20. DMRG results for a horizontal scan through Fig. 1 with $1/U = 2.5$. We consider up to $L = 128$ and extrapolate to the thermodynamic limit. (a) Evolution of the ground state energy E_0 with increasing local Hilbert space restriction, $n_r = n_a = n_m$. (b) Evolution of the excitation gap E_{1g} with increasing n_r , showing very little change beyond $n_r = 5$.

t/U , where inter-site hopping is strongly favored, one should check the validity of this approximation. Here we discuss the evolution of physical observables with increasing Hilbert space restriction parameter, $n_r = n_a = n_m$. For the largest value of $1/U = 2.5$ used in Fig. 1, the results converge with increasing n_r . For example, in Fig. 20(a) we show the evolution of the ground state energy E_0 with increasing n_r . The results show very little variation beyond $n_r = 5$. Likewise, in Fig. 20(b) we monitor the excitation gap E_{1g} with increasing n_r . The data again show very little change beyond $n_r = 5$. The associated MC to AC+MC phase boundary in Fig. 1 is therefore robust to increasing n_r . In a similar fashion, in Figs. 21 and 22, we examine the evolution of the atomic and molecular correlation functions. The results show clear convergence in both the MC and AC+MC phases. The excellent agreement between our DMRG results and field theory predictions also lends *a posteriori* support for this level of Hilbert space restriction with $n_r = 5$.

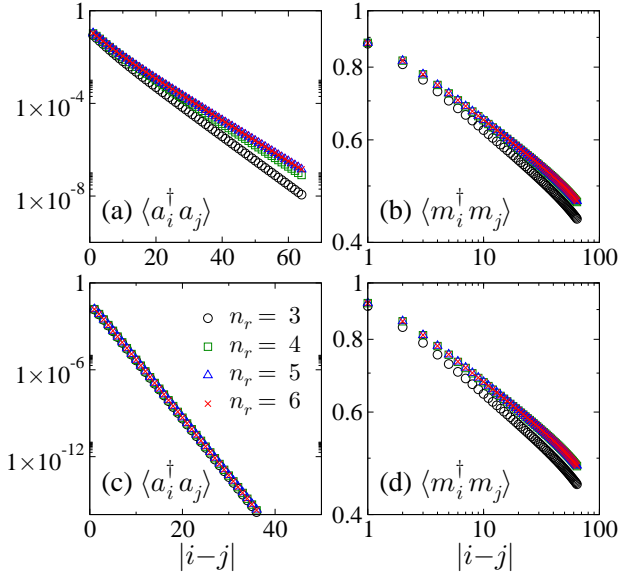


FIG. 21. (color online). DMRG results with $L = 128$ and $U = 0.5$ within the MC phase shown in Fig. 1. We show the evolution of the atomic and molecular correlation functions with increasing local Hilbert space restriction n_r . We set $\epsilon_m = -4$ ($\epsilon_m = -6$) in the upper (lower) panels.

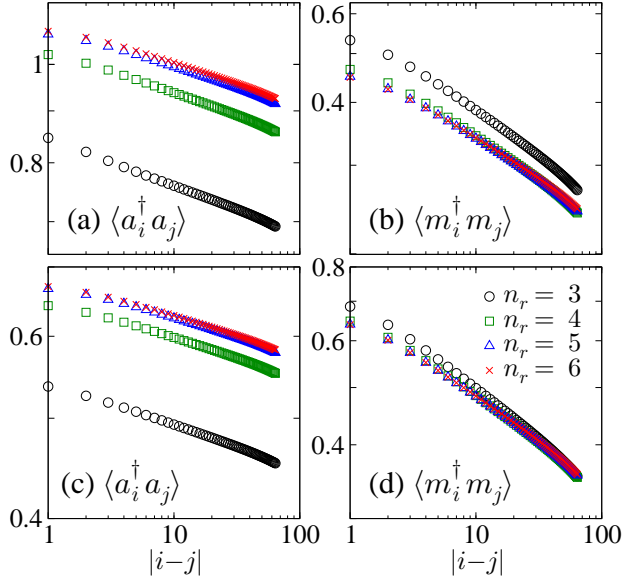


FIG. 22. (color online). DMRG results with $L = 128$ and $U = 0.5$ within the AC+MC phase shown in Fig. 1. We show the evolution of the atomic and molecular correlation functions with increasing local Hilbert space restriction n_r . We set $\epsilon_m = -2$ ($\epsilon_m = -3$) in the upper (lower) panels.

- [1] M. H. Anderson, J. R. Ensher, M. R. Matthews, C. E. Wieman, and E. A. Cornell, *Science*, **269**, 198 (1995).
 [2] K. B. Davis, M.-O. Mewes, M. R. Andrews, N. J. van Druten, D. S. Durfee, D. M. Kurn, and W. Ketterle,

- Phys. Rev. Lett.*, **75**, 3969 (1995).
 [3] M. Greiner, O. Mandel, T. Esslinger, T. W. Hänsch, and I. Bloch, *Nature*, **415**, 39 (2002).

- [4] K. Baumann, C. Guerlin, F. Brennecke, and T. Esslinger, *Nature*, **464**, 1301 (2010).
- [5] D. M. Eagles, *Phys. Rev.*, **186**, 456 (1969).
- [6] A. J. Leggett, *J. Phys. C (Paris)*, **41**, 7 (1980).
- [7] P. Nozières and S. Schmitt-Rink, *J. Low. Temp. Phys.*, **59**, 195 (1985).
- [8] A. J. Leggett, *Quantum Liquids: Bose Condensation and Cooper Pairing in Condensed-Matter Systems* (Oxford University Press, 2006).
- [9] M. Greiner, C. A. Regal, and D. S. Jin, *Nature*, **426**, 537 (2003).
- [10] S. Jochim, M. Bartenstein, A. Altmeyer, G. Hendl, S. Riedl, C. Chin, J. Hecker Denschlag, and R. Grimm, *Science*, **302**, 2101 (2003).
- [11] M. W. Zwierlein, C. A. Stan, C. H. Schunck, S. M. F. Raupach, S. Gupta, Z. Hadzibabic, and W. Ketterle, *Phys. Rev. Lett.*, **91**, 250401 (2003).
- [12] C. A. Regal, M. Greiner, and D. S. Jin, *Phys. Rev. Lett.*, **92**, 040403 (2004).
- [13] T. Bourdel, L. Khaykovich, J. Cubizolles, J. Zhang, F. Chevy, M. Teichmann, L. Tarruell, S. J. J. M. F. Kokkelmans, and C. Salomon, *Phys. Rev. Lett.*, **93**, 050401 (2004).
- [14] M. W. Zwierlein, C. A. Stan, C. H. Schunck, S. M. F. Raupach, A. J. Kerman, and W. Ketterle, *Phys. Rev. Lett.*, **92**, 120403 (2004).
- [15] M. Bartenstein, A. Altmeyer, S. Riedl, S. Jochim, C. Chin, J. Hecker Denschlag, and R. Grimm, *Phys. Rev. Lett.*, **92**, 203201 (2004).
- [16] W. Ketterle and M. W. Zwierlein, in *Ultracold Fermi Gases*, Proceedings of the International School of Physics “Enrico Fermi”, Course CLXIV, Varenna, 2006 (2008).
- [17] S. Ospelkaus, K.-K. Ni, D. Wang, M. H. G. de Miranda, B. Neyenhuis, G. Quémener, P. S. Julienne, J. L. Bohn, D. S. Jin, and J. Ye, *Science*, **327**, 853 (2010).
- [18] S. Inouye, M. R. Andrews, J. Stenger, H.-J. Miesner, D. M. Stamper-Kurn, and W. Ketterle, *Nature*, **392**, 151 (1998).
- [19] Ph. Courteille, R. S. Freeland, D. J. Heinzen, F. A. van Abeelen, and B. J. Verhaar, *Phys. Rev. Lett.*, **81**, 69 (1998).
- [20] E. A. Donley, N. R. Claussen, S. T. Thompson, and C. E. Wieman, *Nature*, **417**, 529 (2002).
- [21] J. Herbig, T. Kraemer, M. Mark, T. Weber, C. Chin, H.-C. Nägerl, and R. Grimm, *Science*, **301**, 1510 (2003).
- [22] S. Dürr, T. Volz, and G. Rempe, *Phys. Rev. A*, **70**, 031601(R) (2004).
- [23] K. Xu, T. Mukaiyama, J.-R. Abo-Shaeer, J. K. Chin, D. E. Miller, and W. Ketterle, *Phys. Rev. Lett.*, **91**, 210402 (2003).
- [24] P. D. Drummond, K. V. Kheruntsyan, and H. He, *Phys. Rev. Lett.*, **81**, 3055 (1998).
- [25] E. Timmermans, P. Tommasini, M. Hussein, and A. Kerman, *Phys. Rep.*, **315**, 199 (1999).
- [26] R. A. Duine and H. T. C. Stoof, *Phys. Rep.*, **396**, 115 (2004).
- [27] S. B. Papp, J. M. Pino, R. J. Wild, S. Ronen, C. E. Wieman, D. S. Jin, and E. A. Cornell, *Phys. Rev. Lett.*, **101**, 135301 (2008).
- [28] S. E. Pollack, D. Dries, M. Junker, Y. P. Chen, T. A. Corcovilos, and R. G. Hulet, *Phys. Rev. Lett.*, **102**, 090402 (2009).
- [29] N. Navon, S. Piatecki, K. Günter, B. Rem, T. C. Nguyen, F. Chevy, W. Krauth, and C. Salomon, *Phys. Rev. Lett.*, **107**, 135301 (2011).
- [30] G. Thalhammer, K. Winkler, F. Lang, S. Schmid, R. Grimm, and J. H. Denschlag, *Phys. Rev. Lett.*, **96**, 050402 (2006).
- [31] C. Chin, R. Grimm, P. Julienne, and E. Tiesinga, *Rev. Mod. Phys.*, **82**, 1225 (2010).
- [32] L. Radzihovsky, J. Park, and P. B. Weichman, *Phys. Rev. Lett.*, **92**, 160402 (2004).
- [33] M. W. J. Romans, R. A. Duine, S. Sachdev, and H. T. C. Stoof, *Phys. Rev. Lett.*, **93**, 020405 (2004).
- [34] L. Radzihovsky, P. B. Weichman, and J. I. Park, *Ann. Phys.*, **323**, 2376 (2008).
- [35] D. B. M. Dickerscheid, U. Al Khawaja, D. van Oosten, and H. T. C. Stoof, *Phys. Rev. A*, **71**, 043604 (2005).
- [36] K. Sengupta and N. Dupuis, *Europhys. Lett.*, **70**, 586 (2005).
- [37] V. G. Rousseau and P. J. H. Denteneer, *Phys. Rev. Lett.*, **102**, 015301 (2009).
- [38] V. G. Rousseau and P. J. H. Denteneer, *Phys. Rev. A*, **77**, 013609 (2008).
- [39] M. J. Bhaseen, A. O. Silver, M. Hohenadler, and B. D. Simons, *Phys. Rev. Lett.*, **103**, 265302 (2009).
- [40] M. Hohenadler, A. O. Silver, M. J. Bhaseen, and B. D. Simons, *Phys. Rev. A*, **82**, 013639 (2010).
- [41] C. Wu, *Phys. Rev. Lett.*, **95**, 266404 (2005).
- [42] P. Lecheminant, E. Boulat, and P. Azaria, *Phys. Rev. Lett.*, **95**, 240402 (2005).
- [43] S. Capponi, G. Roux, P. Azaria, E. Boulat, and P. Lecheminant, *Phys. Rev. B*, **75**, 100503(R) (2007).
- [44] G. Roux, S. Capponi, P. Lecheminant, and P. Azaria, *Eur. Phys. J. B*, **68**, 293 (2009).
- [45] A. J. Daley, J. M. Taylor, S. Diehl, M. Baranov, and P. Zoller, *Phys. Rev. Lett.*, **102**, 040402 (2009).
- [46] A. J. Daley, J. M. Taylor, S. Diehl, M. Baranov, and P. Zoller, *Phys. Rev. Lett.*, **102**, 179902 (2009).
- [47] S. Diehl, M. Baranov, A. J. Daley, and P. Zoller, *Phys. Rev. Lett.*, **104**, 165301 (2010).
- [48] S. Diehl, M. Baranov, A. J. Daley, and P. Zoller, *Phys. Rev. B*, **82**, 064509 (2010).
- [49] S. Diehl, M. Baranov, A. J. Daley, and P. Zoller, *Phys. Rev. B*, **82**, 064510 (2010).
- [50] L. Bonnes and S. Wessel, *Phys. Rev. Lett.*, **106**, 185302 (2011).
- [51] L. Bonnes and S. Wessel, “Half-Vortex Unbinding and Ising Transition in Constrained Superfluids,” arXiv:1201.4117.
- [52] S. R. Manmana, A. M. Läuchli, F. H. L. Essler, and F. Mila, *Phys. Rev. B*, **83**, 184433 (2011).
- [53] Y. Shi, A. Lamacraft, and P. Fendley, “Boson Pairing and Unusual Criticality in a Generalized XY Model,” arXiv:1108.5744.
- [54] S. E. Korshunov, *JETP Lett.*, **41**, 263 (1985), [*Zh. Eksp. Teor. Fiz.* **41** 216 (1985)].
- [55] D. H. Lee and G. Grinstein, *Phys. Rev. Lett.*, **55**, 541 (1985).
- [56] D. B. Carpenter and J. T. Chalker, *J. Phys.: Condens. Mat.*, **1**, 4907 (1989).
- [57] J. G. Valatin and D. Butler, *Nuovo Cimento*, **10**, 37 (1958).
- [58] A. Coniglio and M. Marinaro, *Nuovo Cimento*, **48B**, 249 (1967).
- [59] W. A. B. Evans and Y. Imry, *Nuovo Cimento*, **63B**, 155 (1969).

- [60] P. Nozières and D. Saint James, *J. Phys. France*, **43**, 1133 (1982).
- [61] M. J. Rice and Y. R. Wang, *Phys. Rev. B*, **37**, 5893 (1988).
- [62] M. Yu. Kagan and D. V. Efremov, *Phys. Rev. B*, **65**, 195103 (2002).
- [63] S. Ejima, M. J. Bhaseen, M. Hohenadler, F. H. L. Essler, H. Fehske, and B. D. Simons, *Phys. Rev. Lett.*, **106**, 015303 (2011).
- [64] S. R. White, *Phys. Rev. Lett.*, **69**, 2863 (1992); *Phys. Rev. B*, **48**, 10345 (1993).
- [65] In this 1D setting we use the terms “superfluid” and “condensate” to indicate a phase with power-law correlations.
- [66] L. Radzihovsky and S. Choi, *Phys. Rev. Lett.*, **103**, 095302 (2009).
- [67] S. Choi and L. Radzihovsky, *Phys. Rev. A*, **84**, 043612 (2011).
- [68] R. B. Diener and T.-L. Ho, *Phys. Rev. A*, **73**, 017601 (2006).
- [69] D. B. M. Dickerscheid, D. van Oosten, and H. T. C. Stoof, *Phys. Rev. A*, **73**, 017602 (2006).
- [70] H. P. Büchler, *Phys. Rev. Lett.*, **104**, 090402 (2010).
- [71] M. Eckholt and T. Roscilde, *Phys. Rev. Lett.*, **105**, 199603 (2010).
- [72] Y.-W. Lee and Y.-L. Lee, *Phys. Rev. B*, **70**, 224506 (2004).
- [73] M. Sitte, A. Rosch, J. S. Meyer, K. A. Matveev, and M. Garst, *Phys. Rev. Lett.*, **102**, 176404 (2009).
- [74] V. Gurarie, *Phys. Rev. A*, **73**, 033612 (2006); arXiv:0912.3204.
- [75] Y.-W. Lee and Y.-L. Lee, *Phys. Rev. A*, **73**, 043606 (2006).
- [76] T. T. Wu, B. M. McCoy, C. A. Tracy, and E. Barouch, *Phys. Rev. B*, **13**, 316 (1976).
- [77] J. M. Kosterlitz and D. J. Thouless, *J. Phys. C*, **6**, 1181 (1973).
- [78] J. M. Kosterlitz, *J. Phys. C*, **7**, 1046 (1974).
- [79] T. D. Kühner, S. R. White, and H. Monien, *Phys. Rev. B*, **61**, 12474 (2000).
- [80] T. Giamarchi, *Phys. Rev. B*, **46**, 342 (1992).
- [81] H. P. Büchler, G. Blatter, and W. Zwerger, *Phys. Rev. Lett.*, **90**, 130401 (2003).
- [82] H. G. Vaidya and C. A. Tracy, *Physica A*, **92**, 1 (1978).
- [83] M.-C. Cha, J.-G. Shin, and J.-W. Lee, *Phys. Rev. B*, **80**, 193104 (2009).
- [84] M.-C. Cha, *J. Supercond. Novel Magn.*, **23**, 725 (2010).
- [85] F. Gerbier, A. Widera, S. Fölling, O. Mandel, T. Gericke, and I. Bloch, *Phys. Rev. Lett.*, **95**, 050404 (2005).
- [86] J. Cardy, *Scaling and Renormalization in Statistical Physics* (Cambridge University Press, 1996).
- [87] C. Holzhey, F. Larsen, and F. Wilczek, *Nucl. Phys. B*, **424**, 443 (1994).
- [88] P. Calabrese and J. Cardy, *J. Stat. Mech.*, P06002 (2004).
- [89] P. Calabrese, M. Campostrini, F. H. L. Essler, and B. Nienhuis, *Phys. Rev. Lett.*, **104**, 095701 (2010).
- [90] J. Cardy and P. Calabrese, *J. Stat. Mech.: Theor. Exp.*, P04023 (2010).
- [91] P. Calabrese and F. H. L. Essler, *J. Stat. Mech.: Theor. Exp.*, P08029 (2010).
- [92] J. C. Xavier and F. C. Alcaraz, *Phys. Rev. B*, **83**, 214425 (2011).
- [93] M. Fagotti and P. Calabrese, *J. Stat. Mech.: Theor. Exp.*, P01017 (2011).
- [94] E. Eriksson and H. Johannesson, *J. Stat. Mech.: Theor. Exp.*, P02008 (2011).
- [95] M. Dalmonte, E. Ercolessi, and L. Taddia, *Phys. Rev. B*, **84**, 085110 (2011).
- [96] A. M. Läuchli and C. Kollath, *J. Stat. Mech.*, P05018 (2008).